JGR Space Physics

RESEARCH ARTICLE
10.1029/2023JA032287

Special Section:
Fifteen Years of THEMIS Mission

Relativistic Electron Precipitation Driven by Mesoscale Transients, Inferred From Ground and Multi-Spacecraft Platforms

A. V. Artemyev[1,2], X.-J. Zhang[1,3], A. G. Demekhov[4], X. Meng[5], V. Angelopoulos[1], and Yu. V. Fedorenko[4]

[1]Department of Earth, Planetary, and Space Sciences, University of California, Los Angeles, CA, USA, [2]Space Research Institute of Russian Academy of Sciences, Moscow, Russia, [3]Department of Physics, University of Texas at Dallas, Richardson, TX, USA, [4]Polar Geophysical Institute, Apatity, Russia, [5]Jet Propulsion Laboratory, California Institute of Technology, Pasadena, CA, USA

Key Points:

- We report night-side relativistic electron precipitation associated with whistler-mode waves
- Wave ducting is one possible explanation of the observed precipitating electron spectra
- We examine the role of plasma injections and foreshock transients in relativistic electron losses

Correspondence to:
A. V. Artemyev,
aartemyev@igpp.ucla.edu

Citation:
Artemyev, A. V., Zhang, X.-J., Demekhov, A. G., Meng, X., Angelopoulos, V., & Fedorenko, Y. V. (2024). Relativistic electron precipitation driven by mesoscale transients, inferred from ground and multi-spacecraft platforms. *Journal of Geophysical Research: Space Physics*, *129*, e2023JA032287. https://doi.org/10.1029/2023JA032287

Received 15 NOV 2023
Accepted 9 JAN 2024

Abstract Precipitation of relativistic electrons into the Earth's atmosphere regulates the outer radiation belt fluxes and contributes to magnetosphere-atmosphere coupling. One of the main drivers of such precipitation is electron scattering by whistler-mode waves. Such waves typically originate at the equator, where they can resonate with and scatter sub-relativistic (tens to a few hundred keV) electrons. However, they can occasionally propagate far away from the equator along field lines, reaching middle latitudes, where they can resonate with and scatter relativistic (>500 keV) electrons. Such a propagation is typical for the dayside, but statistically has not been found on the nightside where the waves are quickly damped along their propagation due to Landau damping. Here we explore two events of relativistic electron precipitation from low-altitude observations on the nightside. Combining measurements of whistler-mode waves from ground observatories, relativistic electron precipitation from low-altitude satellites, total electron content maps from GPS receivers, and magnetic field and electron flux from equatorial satellites, we show wave ducting by plasma density gradients is the possible channel that allows the waves to reach middle latitudes and scatter relativistic electrons. We suggest that both whistler-mode wave generation and ducting can be driven by equatorial mesoscale (with spatial scales of about one Earth radius) transient structures during nightside injections. We also compare these nightside events with observations of ducted waves and relativistic electron precipitation at the dayside, where wave generation and ducting are driven by ultra-low-frequency waves. This study demonstrates the potential importance of mesoscale transients in relativistic electron precipitation, but does not however unequivocally establish that ducted whistler-mode waves are the primary cause of the observed electron precipitation.

1. Introduction

Energetic electron precipitation from the outer radiation belt into the Earth's atmosphere is predominantly driven by electron resonant interactions with whistler-mode waves (see reviews by Millan and Thorne (2007), Tsurutani et al. (2013), Li and Hudson (2019), and Thorne et al. (2021)). The characteristics of precipitation events, such as the precipitating electron energy, are dictated by the properties of the waves and of the background plasma and magnetic field. The key characteristic that determines energies of electrons scattered by the most intense, field-aligned waves is the latitudinal distribution of wave intensity (Agapitov et al., 2018; Mourenas et al., 2014; Summers et al., 2007b; D. Wang & Shprits, 2019). At high latitudes, the higher ratio of cyclotron to plasma frequency increases the electron resonance energy with whistler-mode waves, so that relativistic electrons (>500 keV) can be scattered into the loss-cone even though this is not possible for equatorial electrons (Artemyev et al., 2021; L. Chen et al., 2022; Miyoshi et al., 2020, 2021; Shumko et al., 2021; Tsai et al., 2022). Present radiation belt models are empirically parameterized by temporal and spatial averages of wave properties, using multi-year spacecraft observations (e.g., Agapitov et al., 2013; Li, Ma, et al., 2015; Malaspina et al., 2017; Meredith et al., 2012). The use of such averages is justified by the commonly used quasi-linear diffusion theory, which describes wave-particle interactions based on the assumption of a turbulent spectrum of low-amplitude waves, for which the average wave intensity is a sufficiently good measure (Andronov & Trakhtengerts, 1964; Kennel & Engelmann, 1966; Lyons et al., 1972). Transient populations of intense waves that can interact with the electrons nonlinearly, may be smoothed out in such averages and not represented in empirical wave models. However, these intense waves are likely responsible for the most intense precipitation events, such as microburst precipitation (e.g., Breneman et al., 2017; Hikishima et al., 2010; Mozer et al., 2018; O'Brien et al., 2004; Shumko

et al., 2018; Thorne et al., 2005). Modern models of relativistic microburst precipitation suggest that such a high rate of electron scattering can be caused by intense waves that are ducted (propagating along magnetic field-lines) and propagate to middle latitudes (L. Chen et al., 2020, 2022; Miyoshi et al., 2020). In the absence of wave ducting, the whistler-mode waves will usually be damped away from the equator and their intensity at middle/high latitudes is rather weak, which significantly reduces the resultant relativistic electron losses (L. Chen et al., 2021).

Ducted whistler-mode waves are trapped by local plasma density enhancements or depletions (Helliwell, 1965; Karpman & Kaufman, 1982; Laird & Nunn, 1975; Pasmanik & Trakhtengerts, 2005). An important property of ducted whistler-mode waves is their ability to propagate along the field lines away from their equatorial source, to middle and high latitudes, without experiencing much Landau damping (Bell et al., 2002; Bortnik et al., 2007; Maxworth & Golkowski, 2017; Watt et al., 2013) and wave divergence (Shklyar et al., 2004; L. Chen et al., 2013). Therefore, ducted waves *may have* a high wave intensity at mid-to-high latitudes, providing effective scattering and precipitation of relativistic electrons. The most direct evidence of whistler-mode wave ducting is their propagation to the ionosphere and transformation to electromagnetic waves reaching ground-based VLF (very-low frequency) wave receivers (see examples in Manninen et al. (2013), Titova et al. (2015), Martinez-Calderon et al. (2015), and Shiokawa et al. (2017)). Previous ground-based VLF observations (with or without conjugate wave measurements at the equator) have demonstrated that ducted wave propagation is actually common (Demekhov et al., 2020; Martinez-Calderon et al., 2016, 2020; Y. Shen et al., 2021; Titova et al., 2017). Near-equatorial measurements (R. Chen et al., 2021; Hosseini et al., 2021; Ke et al., 2021; Streltsov & Bengtson, 2020) and numerical simulations (Hanzelka & Santolík, 2019; Inan & Bell, 1977; Streltsov & Goyal, 2021; Woodroffe & Streltsov, 2013) of whistler-mode wave propagation around strong plasma density gradients further reveal parameters of wave ducting and ducted wave characteristics. However, neither ground-based nor magnetospheric wave measurements alone can quantify the role of ducted waves in energetic electron scattering and precipitation. To do so, one needs to combine low-altitude spacecraft measurements of precipitating electrons and modeling/observations of ducted waves (e.g., Artemyev et al., 2021; L. Chen et al., 2022).

Because of magnetic mapping uncertainties, however, it is difficult to establish the one-to-one correlation between relativistic electron precipitation at low altitudes and equatorial plasma structures potentially responsible for whistler-mode wave ducting. To resolve this issue, in this paper we project low-altitude precipitation measurements to the ionospheric total electron content (TEC) maps, which can be used to identify magnetospheric plasma boundaries but do not suffer from as large magnetic mapping uncertainties (Belehaki et al., 2004; Heise et al., 2002; Lee et al., 2013; Vo & Foster, 2001; Yizengaw & Moldwin, 2005). We analyze in detail three precipitation events from the Electron Losses and Fields Investigation (ELFIN) CubeSats (Angelopoulos et al., 2020), in conjunction with ducted whistler-mode waves at VLF receivers on the ground (Demekhov et al., 2017; Fedorenko et al., 2014) and TEC maps in the ionosphere. Ground-based wave measurements support that the observed precipitation is likely driven by ducted whistler-mode waves, whereas TEC maps can pinpoint the location of these precipitation events relative to the equatorial projections of magnetospheric plasma boundaries. The rest of this paper is arranged as follows: we start with a description of the available data sets in Section 2, and then analyze the two nighside events (in Sections 3.1 and 3.2), for which the relativistic electron precipitation cannot be described by the near-equatorial field-aligned wave distribution from previous statistics. In Section 3.3, we analyze two possible explanations of the relativistic, night-side precipitation events: whistler-mode wave ducting or resonances with very oblique waves. Then, we compare the nightside events with one dayside event that shows relativistic precipitation and ducted whistler-mode waves (Section 3.4). Finally, in Section 4, we discuss our findings and summarize our conclusions.

2. Data Sets

We have identified a number of relativistic electron precipitation events at ELFIN (see also Tsai et al. (2023)): out of the dozen events, we present here three of them that are in good conjunctions with the ground station measuring waves in the whistler-mode frequency range. The precipitation burst and ground station was only separated by $\leq 5°$ in latitude (longitudinal separation varies from 10° to 40°). This latitudinal/longitudinal separation is within the spatial scales of ducted whistler-mode waves, as inferred from equatorial and ground-based observations, see Titova et al. (2015), Titova et al. (2017), Demekhov et al. (2017), Martinez-Calderon et al. (2016, 2020), and Bezděková et al. (2020). We have marked the locations of the ground station (LOZ) and precipitation bursts in Figures 2, 8, and 12, respectively. For other events with relativistic electron precipitation, the ground-based

observations do not show wave activities either because of a large separation from the ELFIN orbit, or because the waves do not reach the ionosphere, for example, due to partial ducting up to the middle latitudes (see discussions in L. Chen et al., 2022; Y. Shen et al., 2021) or due to oblique propagation (see discussion below).

These three relativistic electron precipitation events were observed by the two identical ELFIN CubeSats (ELFIN-A and ELFIN-B) at ∼440 km altitude (Angelopoulos et al., 2020). Their energetic particle detector measures ∈[50, 6000] keV electron fluxes with energy resolution $\Delta E/E \sim 0.4$ and pitch-angle resolution ∼22.5° (see examples of electron pitch-angle distributions in, e.g., Mourenas et al., 2021; Angelopoulos et al., 2022). There is no proton contamination to the ELFIN electron detector (Angelopoulos et al., 2020), and we only keep those data with >4counts per second at each energy or angular bin. In this study, we define trapped j_{trap} and precipitating j_{prec} electron fluxes as those averaged over the pitch-angles outside and inside the local loss-cone, respectively (see details of this data product and examples in Tsai et al. (2022), X.-J. Zhang et al. (2022), and Mourenas et al. (2021)).

There are only three well-known mechanisms for the relativistic electron scattering and precipitation: scattering due to magnetic field line curvature, resonant scattering by electromagnetic ion cyclotron (EMIC) waves, and resonant scattering by whistler-mode waves. The curvature scattering is characterized by the distinguishing signature of the energy/latitudinal dispersion (see Sergeev et al. (2023) and Wilkins et al. (2023)), which is not observed during the three selected events, so we can exclude curvature scattering as the potential mechanism for the observed precipitation. Moreover, these three events are characterized not only by relativistic electron precipitation (which can alternatively be attributed to electron scattering by electromagnetic ion cyclotron (EMIC) waves; see Grach et al. (2022) and Capannolo et al. (2023)), but also strong precipitation down to 50 keV, well below the lowest energy in electron precipitation driven by EMIC waves (An et al., 2022; Capannolo et al., 2021; Summers & Thorne, 2003). Such a wide energy range of precipitating electrons precludes electron scattering by EMIC waves as a potential mechanism for the observed precipitation. The only mechanism that can be responsible for the dispersionless precipitation of 50 keV–1 MeV electrons is then the electron scattering by whistler-mode waves (Summers et al., 2007a, 2007b); see similar observations by ELFIN in Tsai et al. (2022), Shi et al. (2022b), and X.-J. Zhang et al. (2023). Therefore, we analyze our events by assuming this mechanism as the main candidate for the observed electron precipitation.

For each event, we analyze ground-based measurements of electromagnetic waves in the frequency range $1-10$ kHz from the receiver at Lovozero (LOZ) in north Russia (67.98°N, 35.08°E; $L_{IGRF} \sim 5.54$; see Fedorenko et al. (2014) and Demekhov et al. (2020)). We also use total electron content (TEC) maps provided by MIT Haystack via the Madrigal database (http://cedar.openmadrigal.org; see Rideout and Coster (2006), Coster et al. (2013), and Vierinen et al. (2015)). The spatial resolution of the TEC map is $1° \times 1°$.

During these events, low-altitude and ground-based measurements are further supplemented by equatorial measurements of omnidirectional energetic electron fluxes and background magnetic fields from THEMIS (Angelopoulos, 2008), MMS (Burch et al., 2016), and GOES 16&17 (see description of these instruments in Angelopoulos et al. (2008), Blake et al. (2016), Dichter et al. (2015), Boudouridis et al. (2020), Auster et al. (2008), Russell et al. (2016), and Singer et al. (1996)). For the third event, we also examine <30 keV ion flux measurements from THEMIS in the Earth's foreshock region (see the instrument description in McFadden et al. (2008)). To put the ELFIN measurements into the context of ion precipitation, we use ion measurements from POES/NOAA and MetOp satellites (Evans & Greer, 2004).

3. Event Analysis

3.1. Event #1

The first event, at ∼01:00 UT on 2020-09-26, occurs in the beginning of the recovery phase of a moderate storm (Sym $-H \sim -60$ nT and starts growing), and in the middle of an intense substorm ($AE \sim 800$ nT, around the peak). This complicates the projection of ELFIN orbit to the equatorial plane, especially in the night-side region where substorm dynamics may significantly deform the magnetic field line configuration (Sitnov et al., 2019; Stephens & Sitnov, 2021). Thus, to confirm our speculation about projections of ELFIN observed precipitation bursts relative to the plasma sheet/inner magnetosphere/plasmasphere boundaries, we use the TEC data set (which have much lower uncertainties in projecting to ELFIN observations).

Figures 1a–1c shows an overview of ELFIN A observations during the first event in the post midnight (MLT ∈ [2, 3]) region. Prior to 01:00:20 UT, ELFIN was conjugate to the plasma sheet and measured ≤100 keV isotropic fluxes with $j_{prec}/j_{trap} \sim 1$. Around 01:00:30 UT, ELFIN crossed the low-altitude projection of the transition region between the plasma sheet and the outer radiation belt. This region is characterized by an increase of the minimum energy of isotropic electron flux ($j_{prec}/j_{trap} \sim 1$) with decreasing latitude. This so-called isotropy boundary of electrons of a given energy (the latitude-boundary corresponding to flux isotropy at that fixed energy) is due to electron scattering by the magnetic field line curvature that is only possible at progressively higher energies as the magnetic field strength and curvature radius increase at lower latitudes (Imhof et al., 1977; Sergeev et al., 1998, 2012). Note that while this dispersion is clearly evident in the second night-side event in our study, and a rather common occurrence at midnight (Artemyev, Angelopoulos, et al., 2022; Wilkins et al., 2023), the dispersion is not very clear in Figure 1, likely because it is latitudinally narrow and cannot be well-resolved by the 3s spin period of ELFIN.

After 01:00:40 UT, ELFIN maps to the outer radiation belt, based on its observations of intense fluxes of trapped electrons and transient bursts of precipitation (as evidenced in the precipitation ratio of precipitating to trapped fluxes: $j_{prec}/j_{trap} \in [0.1, 0.3]$) in the energy range <300 keV (during 01:00:40–01:01:10 UT). The precipitation ratio in these events increases with decreasing energy down to ∼50 keV. We conclude that they are most likely produced by whistler-mode wave scattering (see, e.g., Tsai et al., 2022, for examples of simulations of such precipitation events observed by ELFIN).

To reveal the location of whistler-mode wave origin, we compare ELFIN observations and the TEC map. Figure 1e shows the temporal and spatial average of the TEC along the ELFIN orbit. The precipitation burst (shaded in dark blue) occurs right around the strong TEC gradient. Figure 2 further projects the ELFIN orbit on the ionospheric map of TEC (precipitation burst is shown by the trick trace along the track). ELFIN was on the night-side during this event. The TEC along its track is typical for that longitude: at high magnetic latitudes ($\gtrsim 60°$) the TEC is driven by plasma sheet electron precipitation; at lower magnetic latitudes ($\lesssim 55°$) it is due to the dense plasmasphere (Weygand et al., 2021; Yizengaw & Moldwin, 2005). A TEC local minimum at intermediate latitudes is colocated with the mid-altitude ionospheric trough (MIT, see Aa et al., 2020; Carpenter & Lemaire, 2004) which is associated with strong convection electric fields and hot ion precipitation right tailward from the plasmapause (Heilig et al., 2022; Shinbori et al., 2021). Such 2D TEC pictures therefore provide context for the relativistic electron precipitation burst seen by ELFIN at around 01:01:20 UT in this equatorward science-zone traversal. The burst is observed well before the TEC minimum in the MIT and after ELFIN's entry in the inner magnetosphere at 01:01:00 UT (based on the TEC enhancement, likely due to plasma sheet electron precipitation by curvature scattering at the isotropy boundary seen in Figure 1c). At magnetic latitudes corresponding to the outer radiation belt (equatorward from the plasma sheet latitudes) the TEC map shows an enhancement that is localized in both longitudes and latitudes. Right at the high-latitude boundary of this TEC enhancement ELFIN captured the relativistic electron precipitation. Such a localized TEC enhancement may be driven by electron precipitation from the plasma sheet injection region (e.g., Lyons et al., 2016; Zou et al., 2011).

Additional support on the localization of electron precipitation burst relative to the plasma sheet injection region can be derived from comparing ELFIN measurements and NOAA POES/MetOp measurements (Evans & Greer, 2004) of ion precipitating fluxes: latitudinal location of the transition between isotropic (where precipitating-to-trapped flux ratio is about one) and anisotropic ion fluxes at low altitudes is commonly treated as the projection of the inner edge of the ion plasma sheet (see, e.g., Dubyagin et al., 2002, 2018; Sergeev et al., 2012, and references therein), where plasma sheet injections break (e.g., Dubyagin et al., 2011; Sergeev et al., 2011, 2014). Figure 3 shows that the latitudinal range of electron isotropic precipitation (electron plasma sheet) coincides at ELFIN and NOAA 15/MetOp 2, which cross night-side/dawn sector within ±30 min from the ELFIN crossing. This justifies the comparison of ELFIN and NOAA 15, MetOp 2 measurements: the relativistic electron precipitation burst is located right equatorward of the ion isotropy boundary (i.e., the inner edge of the ion plasma sheet as shown in 30–80 keV and 80 − 240 keV proton fluxes), that is, well within the plasma sheet injection region. Moreover, compared to NOAA 15, MetOp 2 captures much more electron precipitation bursts associated with whistler-mode waves (enhancements of electron precipitation fluxes over a broad energy range of >40 keV with transient precipitation bursts in >130 keV electron fluxes; see discussions of such observations in (Y. Chen et al., 2014; Li et al., 2013, 2014)) equatorward of the ion isotropy boundary. Latitudinal distribution of >40 keV electron precipitation is broader at MetOp 2, which also observes >130 keV precipitation bursts at lower latitudes than NOAA 15. This suggests that between NOAA 15 and MetOp 2 observations (note that ELFIN observations

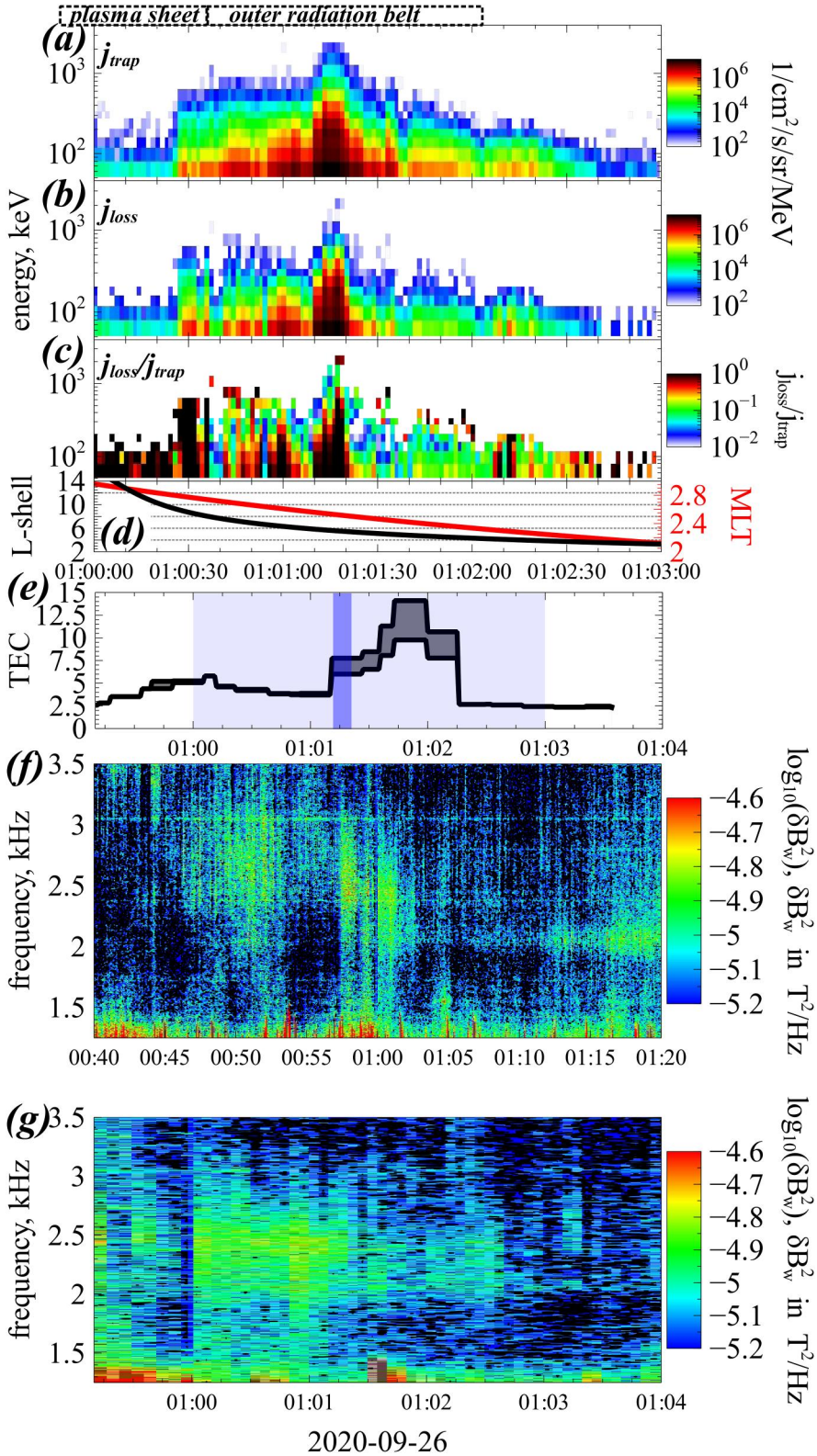

Figure 1.

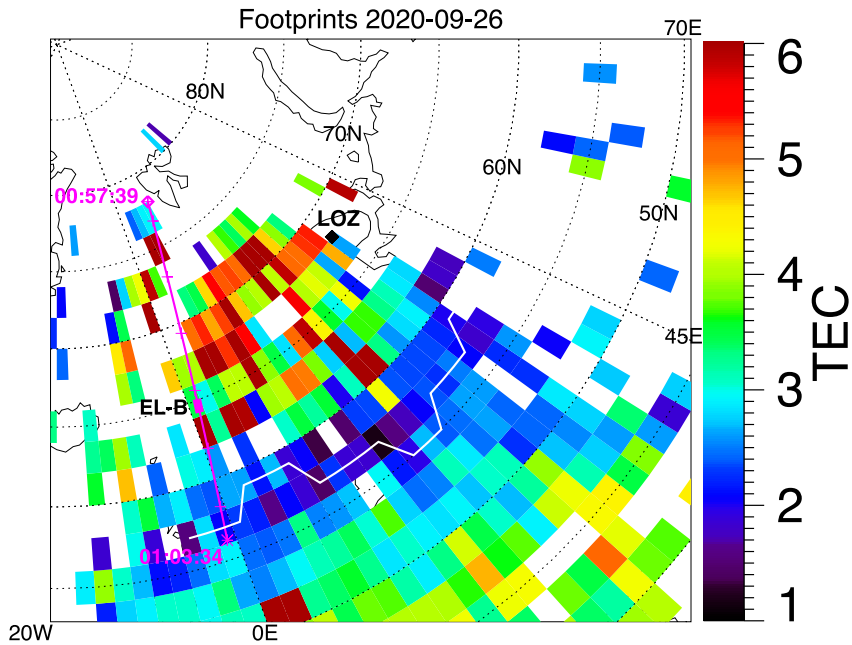

Figure 2. TEC map and ELFIN orbit for the event from Figure 1. Diamonds and asterisks mark the start and end times of the trajectories; crosses are 1 min tickmarks; thick trace denotes times of relativistic electron precipitation identified from Figure 1c. TEC data gaps (due to lack of Global Navigation Satellite System ground receivers) are shown as white. The local TEC minimum associated with the plasmapause (Heilig et al., 2022; Shinbori et al., 2021) is shown by the white curve.

are closer to MetOp 2 observations in time), there was likely a plasma sheet injection that brings hot anisotropic electrons into the outer radiation belt and drives whistler-mode waves and electron precipitation (e.g., Tao et al., 2011; Ukhorskiy et al., 2022).

Although there are no equatorial spacecraft observations in the same MLT sector as ELFIN, the dusk-side equatorial observations suggest that the event #1 occurs right around the time of a plasma injection. Figure 4 shows that MMS, THEMIS, and GOES 16&17 observed several dispersed injections on the dusk flank, at MLT $\in$ [15, 21]. These are likely electron injections that penetrate into the post-midnight inner magnetosphere and reach the spacecraft at pre-midnight, after drifting around the Earth (e.g., Turner et al., 2017). Therefore, Figures 2–4 support the localization of relativistic electron precipitation within the injection region.

3.2. Event #2

The second event, at ~01:00 UT on 2020-09-04, occurs right after the onset of a moderate substorm (peak AE < 500 nT and AE ~ 200 nT during the ELFIN observations). Thus, we may rely on the empirical magnetic field model (Tsyganenko, 1989; Tsyganenko & Sitnov, 2005) for ELFIN projections to the equatorial plane. We also verify this projection using the TEC data set.

Figure 1. Overview plot of 3 minutes of data during the first event. Panels (a), (b), and (c) show ELFIN measurements of trapped fluxes, precipitating fluxes, and precipitating-to-trapped flux ratio. Panel (d) shows ELFIN MLT and *L*-shell derived using the T89 (Tsyganenko, 1989) magnetic model. Note that this event occurs during a moderate storm, when T89 model may not be very accurate. We have thus checked that TS04 (Tsyganenko & Sitnov, 2005) model provides $L \approx 5.5$ instead of $L \approx 6$ of T89 for the main precipitating burst at 01:01:15 UT. Panel (e) shows TEC along the entire, 5 min long date collection, on this ELFIN science zone crossing of the auroral zone and radiation belt: the gray swath bounded by two black lines represents the TEC variation within ±2° around the orbit; the light blue vertical shading marks the time-interval plotted in panels (a–c), and the dark blue shade denotes the time of the relativistic electron precipitation at ELFIN. Panel (f) shows the spectrum of VLF wave measurements at the ground-based station over a much larger, 40 min interval, centered at this ELFIN science zone crossing of interest. Panel (g) shows an expanded view of the VLF wave measurements during the interval from panel (e).

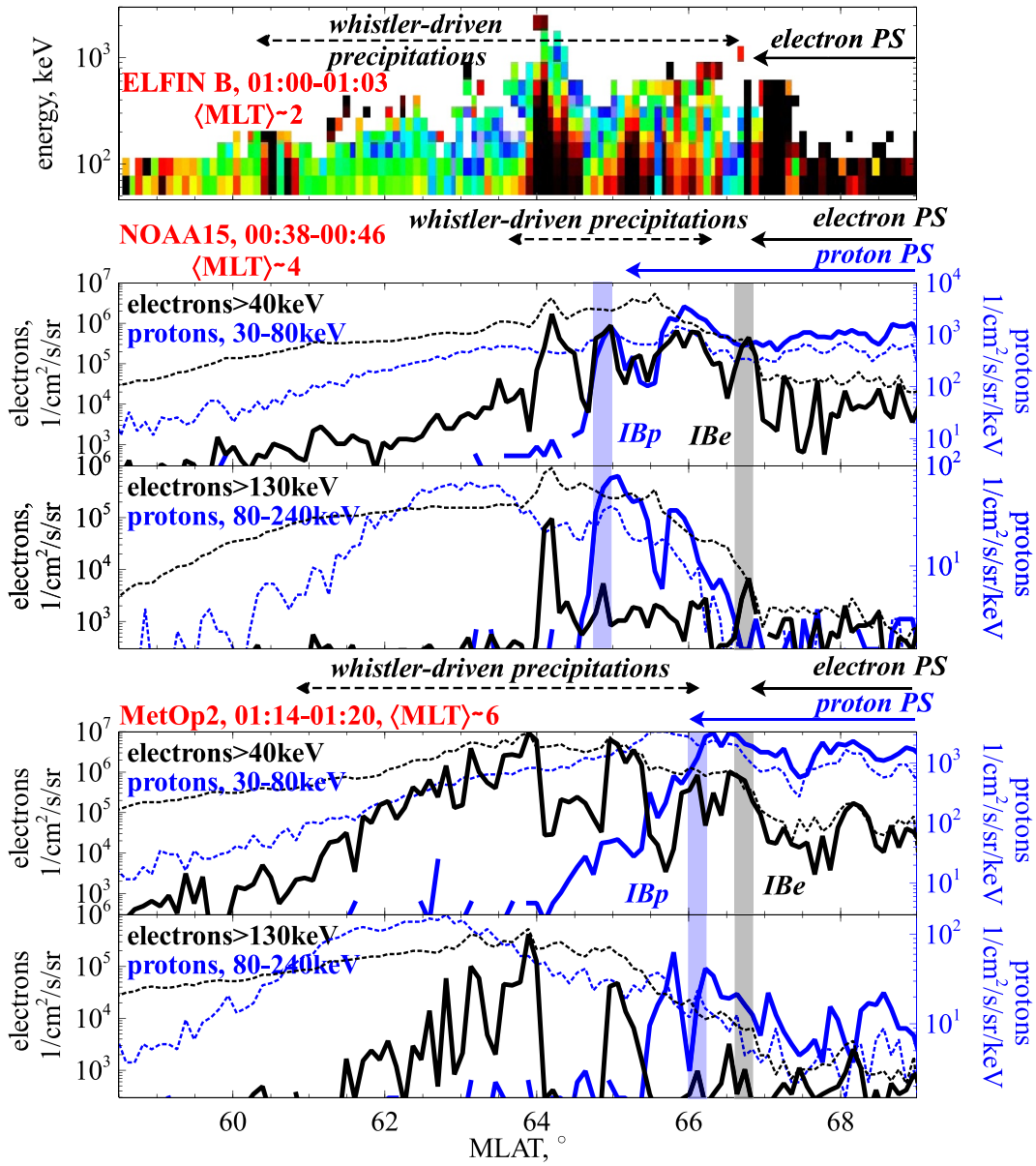

Figure 3. Comparison of ELFIN precipitating-to-trapped flux ratio from Figure 1 and NOAA 15, MetOp-2 observations of precipitating (solid) and trapped (dashed) fluxes of 30 − −80 keV and 80 − 240 keV protons (blue), >40 keV and >13 keV electrons (black). Magnetic latitude calculated from T89 (Tsyganenko, 1989) model is shown in the *x*-axis. ELFIN, NOAA, and MetOp MLT and time intervals are marked in the corresponding panels. Approximate locations of electron (IBe) and proton (IBp) isotropy boundaries are shown by vertical bars; see text for details. Regions of isotropic electron precipitation (electron plasma sheet (PS)) and ion precipitation (ion plasma sheet) are shown by arrows.

Figures 5a–5c shows ELFIN A observations during the second event, which shows similar signatures to the first one: ELFIN observed a burst of relativistic electron precipitation at ∼01:12:22 UT in the night-side inner magnetosphere. The burst occurred in the outer radiation belt (the plasma sheet and the isotropy boundary marking ELFIN's entry into the outer radiation belt can be clearly seen before 01:12:05 UT and within 01:12:05–01:12:20 UT, respectively). During the burst, the precipitating electron energy reaches ∼2 MeV.

To put the ELFIN observations of relativistic electron precipitation bursts into the context of the ion plasma sheet, we compare ELFIN measurements with NOAA 19, 15 data sets that include precipitating ion fluxes. Figure 6 shows that the relativistic electron precipitation burst is observed almost at the ion isotropy boundary (or slightly equatorward of it), which can be identified from equivalent trapped and precipitating proton fluxes at 30 − 80 keV

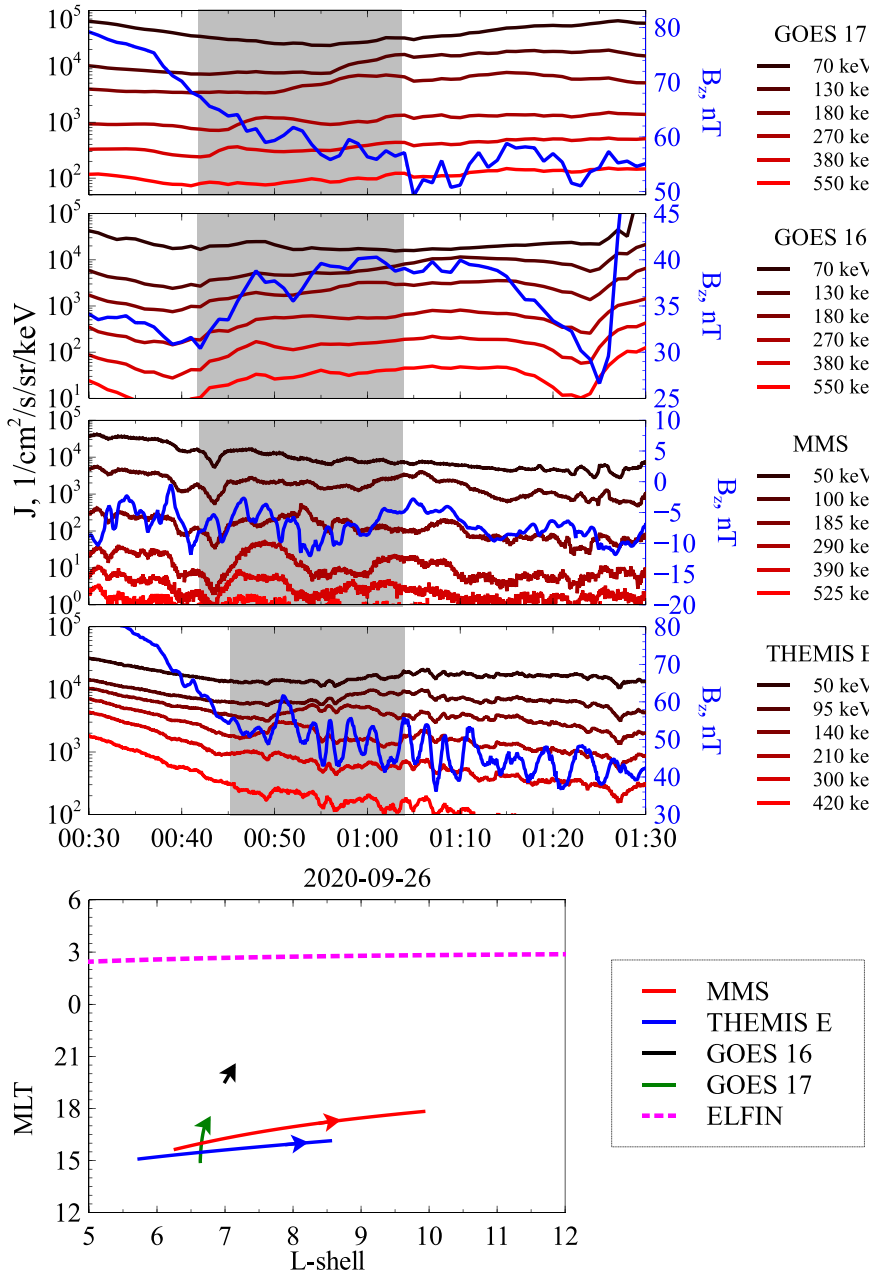

Figure 4. From top to bottom: GOES 17, GOES 16, MMS, and THEMIS E measurements of energetic electron fluxes (reddish traces) and B_z field (blue) during one hour around the first event. The bottom panel shows projections of spacecraft trajectories onto the (L, MLT) plane. Subintervals showing electron flux increases and B_z perturbations likely associated with a plasma injection are shaded in gray.

and 80 − 240 keV. Although NOAA 19, 15 measurements of electron precipitation in the plasma sheet are quite fluctuating and do not allow us to determine the exact position of electron isotropy boundary, the region around and equatorward of the ion isotropy boundary is filled by transient precipitation bursts that are likely driven by whistler-mode waves (see >40 and >130 keV precipitation bursts mostly seen by NOAA 15). Thus, NOAA 19, 15 and ELFIN measurements consistently indicate that relativistic electron precipitation bursts are within the plasma injection region, around the equatorial inner edge of the ion plasma sheet. THEMIS and GOES 16 observations of electron flux increases accompanied by B_z variations around 30 min before ELFIN/NOAA19 orbits also support that the electron precipitation driven by whistler-mode waves is likely generated by the newly

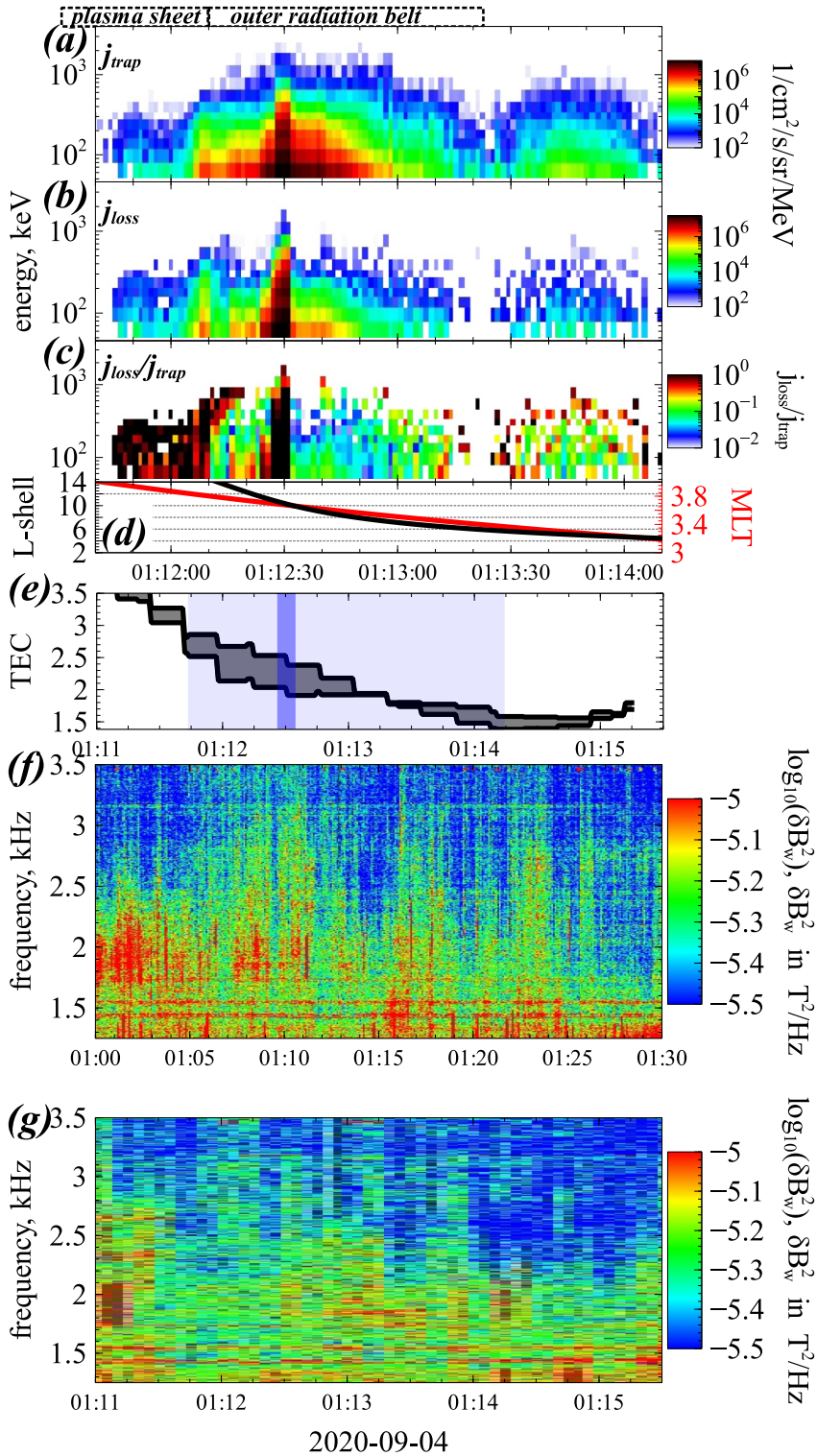

Figure 5. Overview plot of the second event. Panels (a), (b), and (c) show ELFIN measurements of trapped fluxes, precipitating fluxes, and precipitating-to-trapped flux ratio. Panel (d) shows ELFIN MLT and *L*-shell using the T89 (Tsyganenko, 1989) model. Note that this event occurs during a quiet time, when TS04 (Tsyganenko & Sitnov, 2005) and T89 models give the same *L*-shell for the intense precipitation burst at 01:12:25 UT. Panel (e) shows TEC along the ELFIN orbit: the gray color marks TEC variation within ±2° around the orbit, the light blue shade marks the interval from panels (a–c), and the dark blue shade marks the time of the relativistic electron precipitation at ELFIN. Panel (f) shows the spectrum of VLF wave measurements at the ground-based station. Panel (g) shows the expanded view of the VLF wave measurements during the interval from panel (e).

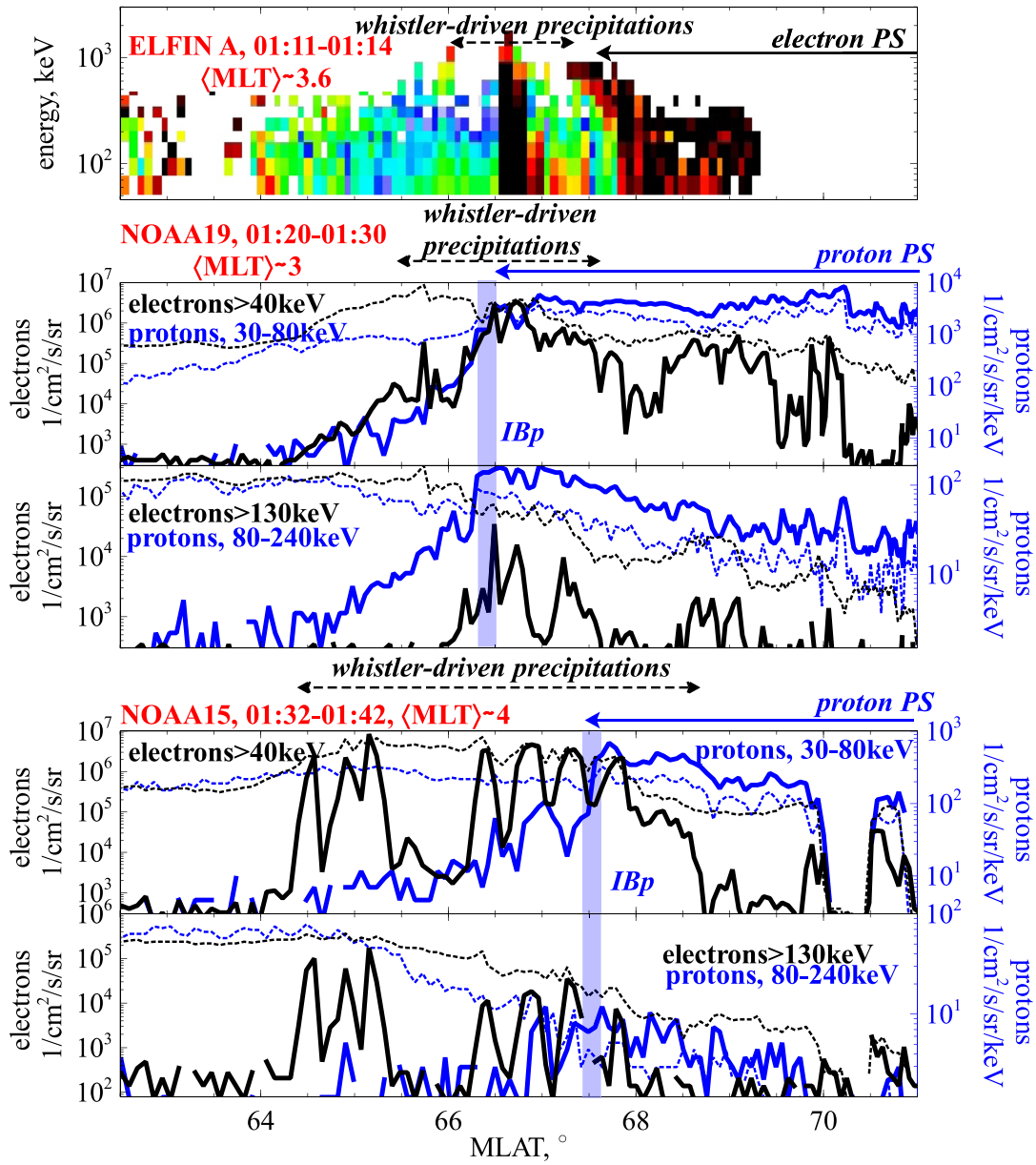

Figure 6. Comparison of ELFIN precipitating-to-trapped flux ratio from Figure 5 and NOAA 19, NOAA 15 observations of precipitating (solid) and trapped (dashed) fluxes of 30 − −80 keV and 80 − 240 keV protons (blue), >40 keV and >13 keV electrons (black). Magnetic latitude calculated from T89 (Tsyganenko, 1989) model is shown in the *x*-axis. ELFIN and NOAA 15, 19 MLT and time intervals are marked in the corresponding panels. Approximate locations of proton (IBp) isotropy boundaries are shown by vertical bars; see text for details. Regions of isotropic ion precipitation (ion plasma sheet) are shown by arrows.

injected, anisotropic electron population (see more discussions in Le Contel et al., 2009; Tao et al., 2011; X. Zhang et al., 2018).

Figure 8 projects the ELFIN orbit to the TEC map (the relativistic electron precipitation is shown in thick traces along the track). Prior to 01:12:00 UT both TEC maps and ELFIN observations are consistent with ELFIN being on plasma sheet field lines (the high TEC is interpreted as due to plasma sheet electron precipitation). The MIT minimum (and the plasmapause; see Shinbori et al. (2021) and Heilig et al. (2022)) occurred around 01:14:00 UT (~60 − 65°). Thus, the relativistic electron precipitation burst is captured by ELFIN between the inner edge of the plasma sheet and the plasmapause, that is, in the outer radiation belt outside the plasmasphere. Intense whistler-

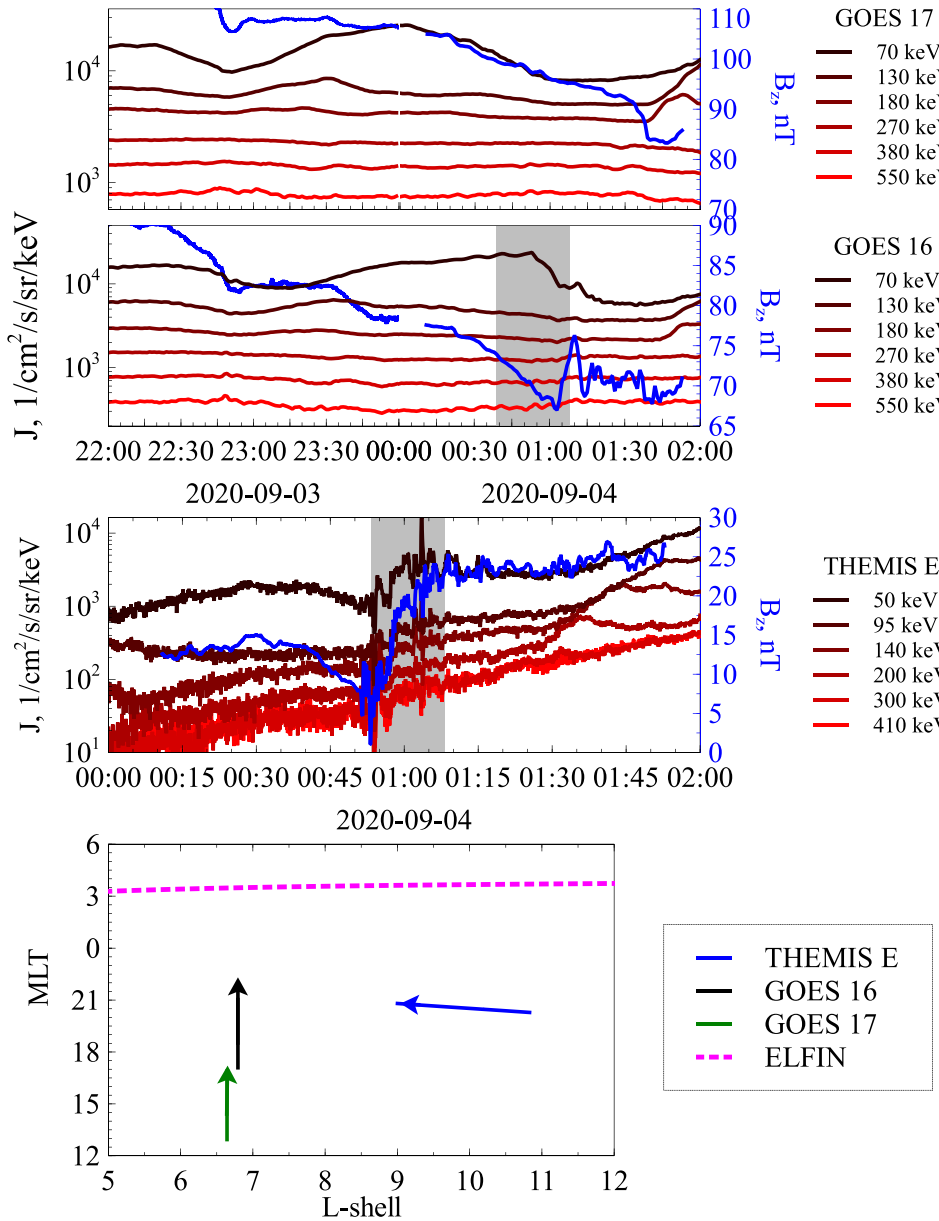

Figure 7. From top to bottom: GOES 17, GOES 16, and THEMIS E measurements of energetic electron fluxes (reddish traces) and B_z field (blue) during two hours centered around the second event. The bottom panel shows projections of spacecraft trajectories onto the (L, MLT) plane. Subintervals showing electron flux increases and B_z perturbations likely associated with a plasma injection are shaded in gray.

mode wave activity within the night-side outer radiation belt are likely associated with the plasma sheet injection. Indeed, THEMIS and GOES 16 captured injections at ~01:00 UT (see Figure 7), whereas the TEC around the ELFIN orbit shows strong variations that are localized in MLT (see Figures 5e and 8). These variations may be due to the TEC increase as a result of plasma sheet electron precipitation from the injection region. Note that ELFIN observations are post-midnight, where injected electrons and the whistler-mode wave source region can drift to from the original injection region at pre-midnight (Tao et al., 2011). This may explain the absence of strong TEC gradients during this event (in comparison with the first event) potentially associated with ELFIN directly traversing the injection region.

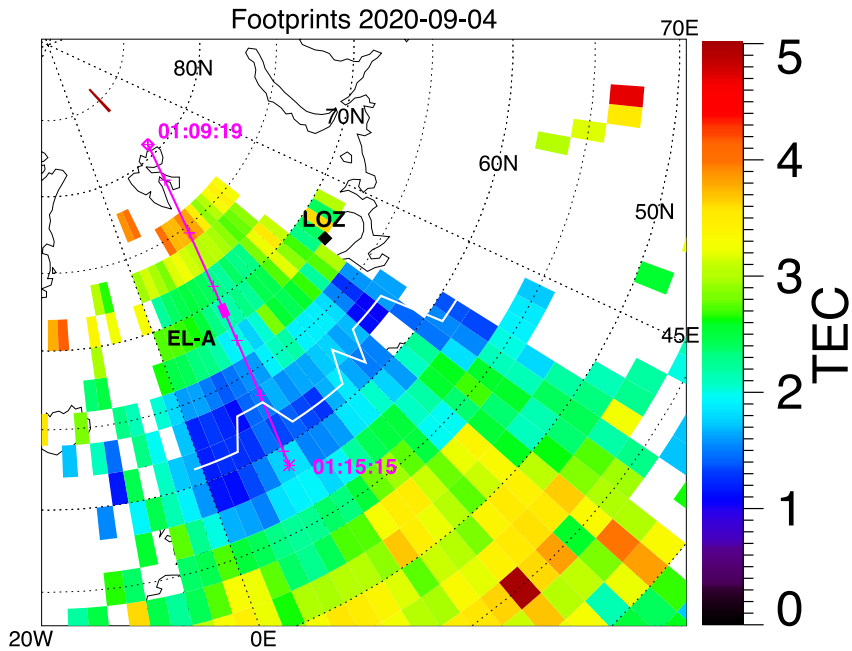

Figure 8. TEC map and the projected ELFIN orbit for the event from Figure 5. Diamonds and asterisks mark the start and end times of the trajectories; crosses are 1 min tickmarks; thick trace denotes times of relativistic electron precipitation identified from Figure 5c. TEC data gaps (due to lack of Global Navigation Satellite System ground receivers) are shown as white. The local TEC minimum associated with the plasmapause (Heilig et al., 2022; Shinbori et al., 2021) is shown by the white curve.

3.3. Two Possible Explanations of the Relativistic Electron Precipitation

Both events #1, 2 show precipitation of electrons over a very wide energy range, 50 keV–1 MeV. Let us discuss two possible mechanisms for such precipitation as observed by ELFIN, in conjunction with wave observations on the ground.

3.3.1. Event #1

For a fixed whistler-mode wave frequency and field-aligned wave propagation, the upper energy limit for electron precipitation largely depends on the maximum latitudinal extent of the wave intensity. Statistical wave distribution models suggest that in the night-side inner magnetosphere, whistler-mode waves are confined below 20° of magnetic latitude (Agapitov et al., 2013; Meredith et al., 2012), and thus usually scatter <300 keV electrons for typical wave frequencies (∼0.35 of equatorial electron gyrofrequency) and cold plasma densities from empirical models (see, e.g., discussion in Artemyev et al., 2021; Artemyev, Zhang, et al., 2022; Tsai et al., 2023). During event #1 (around 01:01:10–01:01:20 UT on 2020-09-26), the electron precipitation up to ∼1 MeV, therefore, implies a much wider latitudinal distribution than statistical models, if we assume the precipitation to be caused by field-aligned whistler-mode wave scattering. Figure 9 further quantifies this discrepancy, by showing that the precipitating-to-trapped flux ratio at ELFIN (the black curve in Panel (c)) remains high at resonant energies corresponding to latitudes where field-aligned whistler-mode wave power distributions (Agapitov et al., 2018) exhibit a significant decrease (Panel (b)). One possible explanation of this discrepancy is that wave ducting during this event enables the waves to propagate to higher latitudes (mid-latitudes, around $\sim 30-40°$) than statistical models (Panel (a) in Figure 9). Indeed, the ground-based VLF receiver conjugate to ELFIN did measure waves in the whistler-mode frequency range, implying that the waves in our event were able to propagate to higher latitudes, reach the ionosphere and the ground. This is evident in Figure 1f, which shows 40 min of ground-based VLF measurements (see also panel (g) with expanded timescale of the VLF wave interval). There is a weak, but clear signal at $f \in [1.5, 3]$kHz, which corresponds to $f/f_{ce} \in [0.27, 0.55]$ for the equatorial f_{ce} expected at $L \approx 5.5$ (the approximate L-shell where ELFIN observed the relativistic electron precipitation). Therefore, both the precipitating energies at ELFIN and VLF measurements on the ground suggest that the strong precipitation burst at 01:01:10–01:01:20 UT may be associated with ducting of the magnetospheric whistler-mode waves. Note that in contrast to the most evidently correlated whistler-mode wave observations at the equator and on the ground

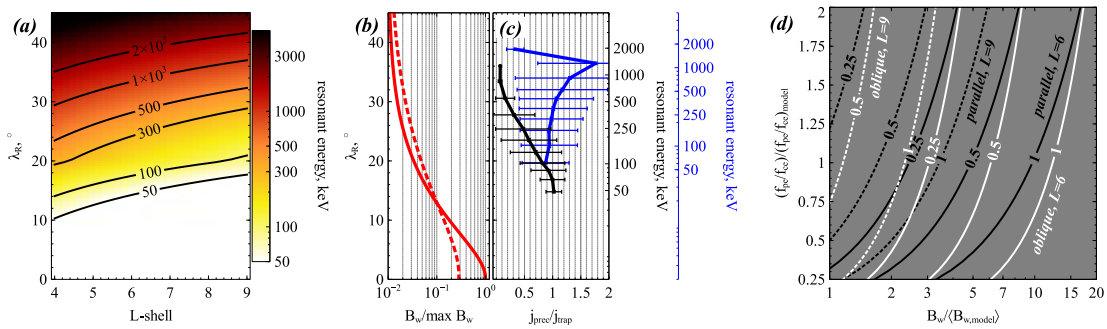

Figure 9. (a) Minimum electron resonance energy as a function of magnetic latitude and *L*-shell using the Sheeley et al. (2001) and Denton et al. (2006) density models and the Agapitov et al. (2018) wave frequency model. (b) Night-side wave intensity distribution as a function of latitude from Agapitov et al. (2018). Solid and dashed curves are profiles for strong and moderate geomagnetic activities, respectively. Both distributions are normalized to the equatorial value, that for strong activity. (c) Precipitating-to-trapped flux ratio (averaged ELFIN data over several spins) as a function of resonant latitude (the latitude where plasma conditions are consistent with minimum resonance energy for that ratio; based on the energy-latitude relationship shown in panel (a)), Black curve shows results for the first event (of Figure 1) and blue curve for the second event (of Figure 5). (d) Contour lines show the f_{pe}/f_{ce} ratio, normalized to the one from Sheeley et al. (2001) model, and wave amplitude, normalized to the value from Agapitov et al. (2018) model, corresponding to different magnitudes of precipitating-to-trapped flux ratio (numbers shown on the figure) for 1 MeV electrons. We show results for two *L*-shell values (corresponding to events from Figures 1 and 5, respectively: solid lines for $L = 6$ and dotted lines for $L = 9$) and two whistler modes: field-aligned waves (black lines) and very oblique waves (white lines); see text for details.

(e.g., Demekhov et al., 2020; Martinez-Calderon et al., 2020; Titova et al., 2017), we do not have measurements of individual wave elements during this event. Instead, the ground-based measurements show a significantly higher wave intensity than the background level over the whistler-mode frequency range. Moreover, these waves are clearly right-hand polarized, with a well-defined polarization ellipse (not shown). These wave signals at the ground-based VLF receiver clearly manifest whistler-mode waves arriving from the magnetosphere (the ground-based VLF transmitters operate at much higher frequencies, have narrowband spectra, and thus cannot contribute to these signals; see Ma et al., 2017; Meredith et al., 2019; Z. Zhang et al., 2018).

The second possible explanation of the observed [50, 1000] keV electron precipitation is the electron resonant interaction with very oblique whistler-mode waves (such an interaction includes high-order resonances that significantly increase the scattering efficiency of relativistic electrons, see, e.g. Lorentzen et al., 2001; Mourenas et al., 2014). Comparison of the precipitation spectra for events conjugate to very oblique waves at the equator (Gan et al., 2023; X.-J. Zhang, Artemyev, et al., 2022) and events conjugate to field-aligned (and most likely ducted) waves (L. Chen et al., 2022) shows that oblique waves usually provide quite small precipitating-to-trapped flux ratios at >0.5 MeV, which is not the case in our events. However, we cannot fully exclude the possibility that such oblique waves are responsible for the very effective precipitation of relativistic electrons as shown in Figure 1. We perform a simple comparison of the expected very oblique and field-aligned wave characteristics, as required by the high precipitating-to-trapped flux ratio (about one) at 1 MeV. We adopt analytical models of bounce-averaged diffusion rates based on the empirical wave model (Agapitov et al., 2018) for field-aligned and very oblique waves (Artemyev et al., 2013; Mourenas et al., 2014). Then the diffusion rates are converted to the precipitating-to-trapped flux ratio following equations from Kennel and Petschek (1966). Figure 9 shows the precipitating-to-trapped flux ratio in the space of wave amplitude (normalized to the model wave intensity) and f_{pe}/f_{ce} (plasma frequency to gyrofrequency at the equator) normalized to the ratio derived from (Sheeley et al., 2001) model. For the event from Figure 1, at *L*-shell ≈6, the wave amplitude should be increased by a factor of $\times 5 - 10$ to provide the observed precipitating-to-trapped flux ratio via scattering either by field-aligned or very oblique waves for the f_{pe}/f_{ce} from (Sheeley et al., 2001) model. However, a lower f_{pe}/f_{ce} will reduce the required wave intensity, to a larger extent for field-aligned waves. Therefore, Figure 9c demonstrates that the observed strong precipitation of relativistic electrons requires unusually large wave intensity or low f_{pe}/f_{ce} (note that such a low f_{pe}/f_{ce} is associated with substorm activity in the nightside and often correlated with whistler-mode wave enhancements, see Agapitov et al., 2019).

As shown in Figures 3 and 4, low-altitude measurements from POES and near-equatorial measurements from THEMIS, GOES, MMS suggest that the relativistic electron precipitation is associated with the plasma sheet injection. An important characteristic of such injections is the plasma density gradient, usually observed at the injection front (e.g., Gkioulidou et al., 2015; Liu et al., 2016), which separated hot, rarefied injected plasma from

the dense ambient plasma (e.g., Sergeev et al., 2009; Vasko et al., 2017). This plasma density gradient may duct intense whistler-mode waves around plasma injections (e.g., Breuillard et al., 2016; Deng et al., 2010; Le Contel et al., 2009). Such a combination will greatly enhance relativistic electron scattering at middle latitudes: plasma injections transport hot, transversely anisotropic electrons, which generate whistler-mode waves (see Tao et al. (2011) and X. Zhang et al. (2018)) and the associated plasma density gradient (injection fronts are characterized by strong Hall fields that move ambient plasma ahead of the front and generate cross-front plasma gradients, see Sergeev et al. (2009) and Runov et al. (2009, 2011)) may serve as a viable channel to duct whistlers to middle latitudes. Note that the proposed mechanism cannot be fully supported by observations shown in Figure 4, because of (a) the large distance (several hours in MLT) between near-equatorial and ELFIN observations, (b) the absence of direct measurements of anisotropic electrons around the equatorial projection of ELFIN. Therefore, this is prospective, but yet to be verified by more fortunate conjunctions between near-equatorial, low-altitude, and ground-based measurements (see, e.g., Artemyev, Neishtadt, & Angelopoulos, 2022, for analysis of ELFIN-THEMIS conjunctions during plasma injections). Moreover, it has been proposed that intense very-oblique waves (also observed in the radiation belts, see Cully et al., 2008; C. Cattell et al., 2008; C. A. Cattell et al., 2015; Agapitov et al., 2014) are likely correlated with plasma sheet injections (Artemyev & Mourenas, 2020; Mourenas et al., 2015), but this remains to be fully verified. Therefore, further investigations are needed to demonstrate the efficiency of very oblique waves in producing strong, bursty precipitation of ∼1 MeV electrons with the precipitating-to-trapped flux ratio about one.

3.3.2. Event #2

Figure 5 shows a relativistic electron precipitation burst likely produced by electron scattering due to whistler-mode waves, because the precipitation extends over a very large energy range, from ∼2 MeV to 50 keV (precipitation of these energies are well correlated with near-equatorial whistler-mode waves, see Y. Chen et al., 2014; Li et al., 2013, 2014). Relativistic electrons can resonate with field-aligned whistler-mode waves if these waves propagate well above the equator, reaching latitudes at or above 30° (see the blue curve in Figure 9c). Curiously, at such latitudes, whistler-mode wave power is rather low at the nightside, according to statistical models of the wave power distribution (see Figures 9b and Meredith et al. (2012); Agapitov et al. (2018)). Yet the observed precipitation at ELFIN is quite intense and transient: there exist flux variations on sub-spin scales (<3s), which cause the precipitating-to-trapped flux ratio to increase above one due to temporal aliasing or nonlinear effects (see more examples and explanation of such large flux ratio measurements in X.-J. Zhang, Angelopoulos, et al., 2022). Therefore, similar to the first event, we shall consider two possible explanations for the electron precipitation. The first interpretation suggests that the observed precipitation of 2 MeV electrons, which can resonate with field-aligned whistler-mode waves only at middle latitudes, indicate wave ducting. And indeed, the ground-based VLF receiver conjugate to ELFIN during this event confirms that $f \sim 1.5$ 2.5 kHz whistler-mode waves reach the ionosphere (Panels (f,g)). Note that the ELFIN L-shell derived from (Tsyganenko, 1989) model may not be accurate, because ELFIN observations are right after a strong substorm injection and dipolarization (see Figure 7 with THEMIS and GOES16&17 observations in the pre-midnight sector). The measured VLF waves are significantly higher than the background and have a well-defined polarization ellipse (not shown). These waves are likely whistler-mode waves arriving from the magnetosphere, because waves generated by VLF transmitters would be observed at much higher frequencies (e.g., Ma et al., 2017; Meredith et al., 2019; Z. Zhang et al., 2018).

Similar to the first event, the low-altitude measurements from POES and near-equatorial measurements from THEMIS, GOES (see Figures 6 and 7) indicate a possible correlation between the relativistic electron precipitation burst and the plasma sheet injection. Therefore, this precipitation burst may be produced by intense, field-aligned whistler-mode waves that are ducted by the plasma density gradient at the injection front and propagate to middle latitudes (the first possible mechanism). Alternatively, as suggested by the second explanation, the relativistic electron precipitation burst may be produced by electron scattering due to very oblique whistler-mode waves (see Figure 9). There are sufficient observational evidences for either one of these two mechanisms, and further numerical simulations and theoretical models are needed to either support the field-aligned wave ducting or the generation of very oblique waves within the plasma injection region.

3.4. Event #3

The third event, at ∼08:40 UT on 2020-11-22, occurs in the middle of a prolonged interval with moderate geomagnetic activities (Sym $-$ H is around -30 nT and AE $\in$ [300, 600] nT during the entire day) driven by the

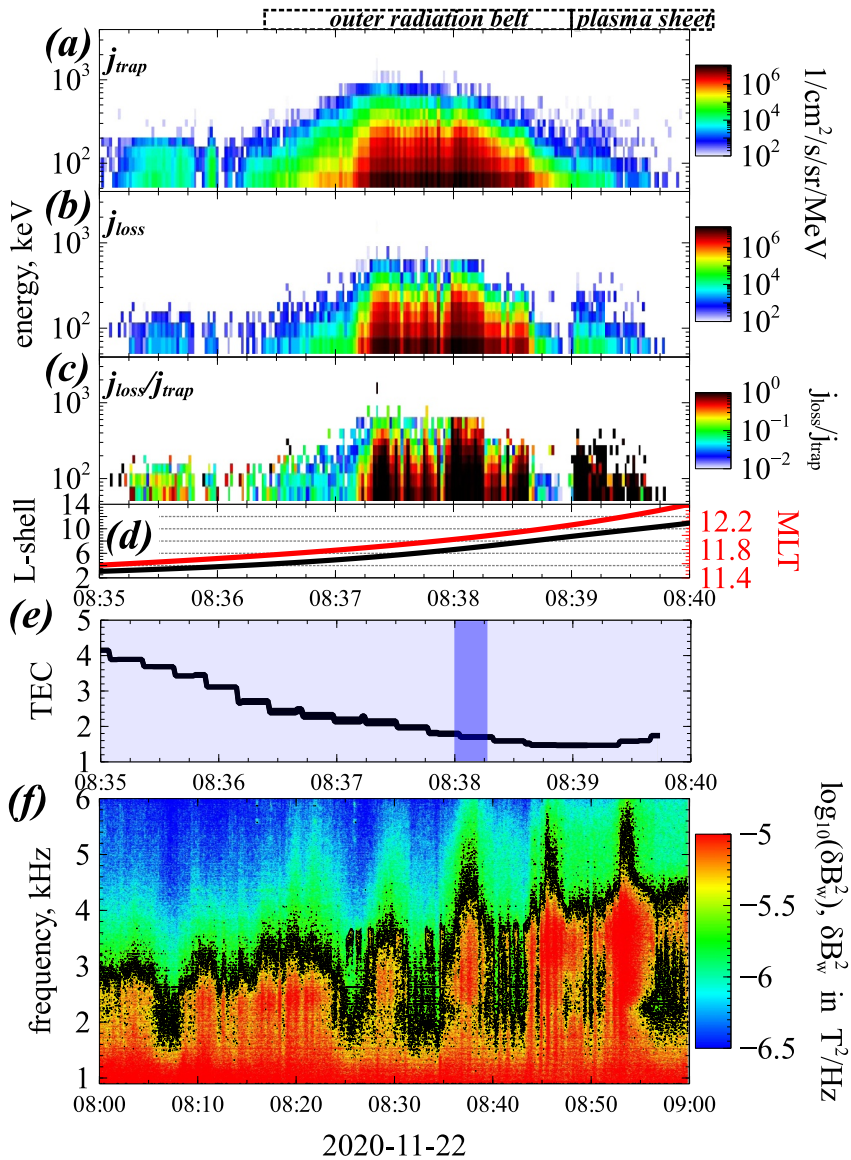

Figure 10. Overview of the third event of a relativistic electron precipitation burst. Panels (a), (b), and (c) show ELFIN measurements of trapped fluxes, precipitating fluxes, and precipitating-to-trapped flux ratio. Panel (d) shows ELFIN MLT and *L*-shell using the T89 (Tsyganenko, 1989) model. Panel (e) shows TEC along the ELFIN orbit: gray shading represents the TEC variation within ±2° around the orbit; light blue vertical shading denotes the time interval plotted in Panels (a–c); dark blue shading depicts the time of the relativistic electron precipitation burst. Panel (f) depicts the spectrum of VLF wave measurements at the ground-based station.

fast solar wind (velocity increases to 500 km/s and dynamical pressure reaches ~5 nPa at the beginning of the day). ELFIN observations are around the noon, where solar wind compression likely deforms magnetic field lines and may provide additional uncertainties for projecting ELFIN observations to the equatorial plane. Thus, to verify our speculations about the ELFIN location relative to the plasmapause, we use TEC data set.

Figures 10a–10c shows ELFIN A measurements for the third event: ELFIN moved from lower *L* to higher *L*, and observed isotropic electron fluxes at <300 keV after 08:39:00 UT. ELFIN mapped to $L > 9$ there (using the T96 (Tsyganenko, 1995) magnetic field model), and thus this isotropic precipitation is likely due to dayside plasma sheet electrons scattered at high *L*. Although no curvature scattering is expected at the dayside, where the magnetic field is only weakly curved, transversely anisotropic hot electrons are often seen at the dayside due to solar wind compression, and such anisotropy can generate intense whistler-mode waves (Li, Thorne, et al., 2015). Thus, we can surmise that ELFIN A's observed electron precipitation after 08:39:00 UT was likely driven by

strong whistler-mode waves at the dayside plasma sheet region (the small equatorial loss-cone size at $L > 9$ can easily result in electron scattering at the strong diffusion and lead to isotropic fluxes, see Kennel (1969)).

Between 08:37:00 UT and 08:39:00 UT, ELFIN maps to the outer radiation belt with high fluxes of trapped electrons. Within this region ELFIN detected several bursts of electron precipitation. The strongest bursts are observed at 08:38:00–08:38:15 UT, where precipitating fluxes approach the levels of trapped fluxes over nearly the entire energy range as evidenced by the flux ratio attaining values near unity (note there are no precipitations above 700 keV likely because there are no trapped fluxes to be scattered by whistler-mode waves). Precipitation bursts before 08:38:00 UT and after 08:38:25 UT are weaker: the precipitating-to-trapped flux ratio is high only up to an upper energy around $\sim 300 - 400$ keV.

The quasi-periodicity of precipitating electron bursts can be explained by the spatial and temporal periodicity of whistler-mode wave sources modulated by dayside compressional ultra-low-frequency (ULF) waves (e.g., Artemyev et al., 2021; X. J. Zhang et al., 2020; X.-J. Zhang et al., 2023; Shi et al., 2022a). Indeed, ground-based VLF receiver at LOZ detected such periodic waves in the whistler-mode frequency range (see Figure 10f). At the VLF receiver, the wave frequency increases with time, that is, the wave frequency increases in the source region conjugate to the receiver. Taking into account that whistler-mode waves are usually generated at the equator with $f/f_{ce} \in [0.2, 0.4]$ (see the latitudinal distribution of f in Agapitov et al., 2018), the observed wave frequency increase indicates an increase of f_{ce} in the conjugate equatorial region. This increase is likely because of the continuous magnetic field compression by the solar wind with the progressively earthward motion of the whistler-mode generation region. During this interval, THEMIS captured quasi-periodic foreshock transients on the dayside: magnetic field perturbations and ion spectrum thermalization (see Figure 11). Such transients are known to drive ULF waves and compression of the magnetosphere (see Hartinger et al., 2013; Hartinger et al., 2014).

Therefore, Figure 10 consistently shows spatially periodic precipitation bursts, likely as a result of periodic whistler-mode wave emissions propagating to the ionosphere. For the most intense precipitation burst at 08:38:00–08:38:25 UT, energies of the measured electron precipitation do not require wave ducting. This is because <700 keV electrons can be scattered by the dayside whistler-mode waves that typically spread along magnetic field lines up to 40° latitudes (Agapitov et al., 2013; Meredith et al., 2012). However, the presence of whistler waves at the conjugate ground-based VLF receiver demonstrates that wave ducting actually does occur. Thus we are compelled to consider how such ducting contributes to the most intense precipitation burst. Projection of this burst to the TEC map (Figure 12) shows that it too coincides with a local minimum of TEC. On this poleward ELFIN orbit, prior to 08:38:00 UT, the TEC increases toward lower L-shells, consistent with the equatorial cold density increase from the plasmasheet to the plasmapause (Sheeley et al., 2001). After 08:38:30 UT, the TEC along the ELFIN orbit slightly increases toward higher L-shells, likely due to the enhanced electron precipitation at the plasma sheet (although due to the absence of TEC coverage and a weak plasma sheet precipitation at the dusk flank, this TEC increase is almost indistinguishable). Therefore, the projection of ELFIN onto the TEC map shows that the most intense relativistic electron precipitation burst is associated with the boundary between the plasma sheet (filled by hot, rarefied electrons) and the inner magnetosphere (filled by cold, dense electrons). The plasma density gradient at this boundary layer are sustained by high-amplitude, ultra-low-frequency waves, and these gradients may duct whistler-mode waves, facilitating their propagation to the ground-based VLF receiver. Wave ducting provides an almost high wave intensity up to high latitudes, which may explain the constant precipitating-to-trapped flux ratio during this precipitation burst.

4. Discussion and Conclusions

In this study we analyze three events of strong relativistic electron precipitation observed by ELFIN: two on the night-side and one on the dayside. The energies of the precipitating electrons range from 50 keV to a 1–2 MeV, suggesting that these electrons were scattered into the loss-cone via resonant interactions with whistler-mode waves. There are two scenarios for whistler-mode waves to scatter relativistic electrons: field-aligned wave ducting to the middle latitudes (Miyoshi et al., 2020; L. Chen et al., 2022) and near-equatorial electron scattering by very oblique waves (Lorentzen et al., 2001).

All three events are associated with ground-based observations of VLF waves, supporting the first explanation of whistler-mode waves ducting. The two night-side relativistic electron precipitation events map magnetically to latitudes between the localized TEC minimum at lower latitudes (the MIT region associated with the plasmapause location (Heilig et al., 2022; Shinbori et al., 2021; Weygand et al., 2021; Yizengaw & Moldwin, 2005)) and the

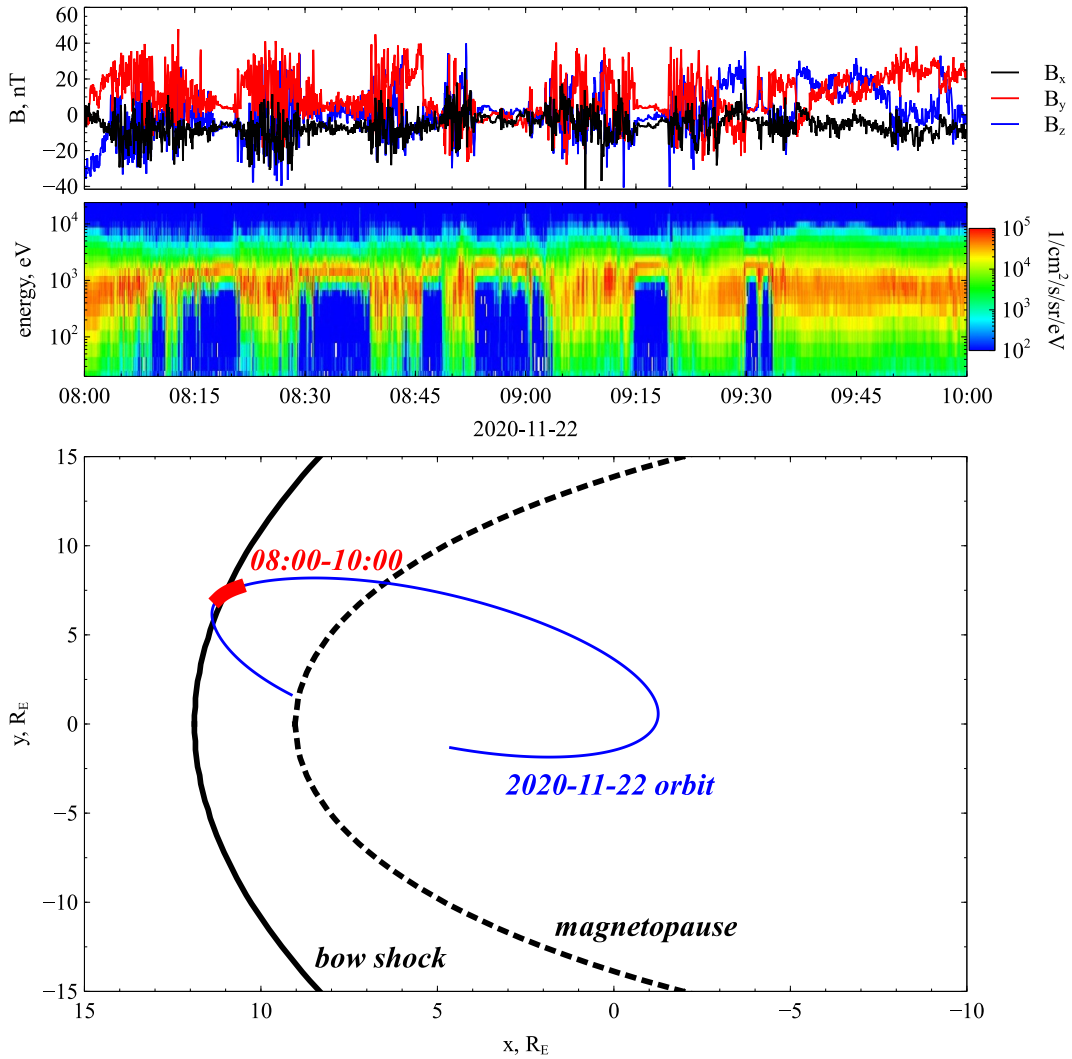

Figure 11. THEMIS observations at the foreshock: (a) magnetic field, (b) ion energy spectrum, (c) THEMIS location relative to the modeled magnetopause (Shue et al., 1997) and bow shock (Wu et al., 2000) locations.

TEC enhancement at higher latitudes due to plasma sheet electron precipitation. Combining with ELFIN measurements of the flux anisotropy (precipitating-to-trapped flux ratio) around the precipitation bursts, we can speculate that these bursts occur between the middle of the outer radiation belt (on the lower latitude side) and just earthward of the inner edge of the plasma sheet (on the higher latitude side). Thus, these precipitation bursts are observed well outside the plasmasphere, which likely excludes the plasmapause (Inan & Bell, 1977; R. Chen et al., 2021) as a candidate for wave ducts during these events. As in the two night-side events, the precipitation occurred after substorm injections, and this may explain both the generation and ducting of intense whistler-mode waves. Injections can transport hot, transversely anisotropic electrons (Fu et al., 2014; Motoba et al., 2020; Tao et al., 2011) and host wave generation sources (Le Contel et al., 2009; Deng et al., 2010; Breuillard et al., 2016; X. Zhang et al., 2018), whereas the injection front separates the background dense plasma front the rarefied plasma from the middle tail reconnection (e.g., Runov et al., 2011, 2015; Sergeev et al., 2009). Density variations across the front are often ≥50% (Runov et al., 2011), which well exceeds the threshold of density variation for whistler-mode wave ducting (e.g., Williams & Streltsov, 2021, and references therein). Therefore, plasma injections that penetrate into the inner magnetosphere and break there can form a short-living, spatially localized region for intense whistler-mode generation and ducting. This region is seen by ELFIN as a burst of relativistic electron precipitation. Most plasma sheet injections will break before reaching the geostationary orbit, well before the

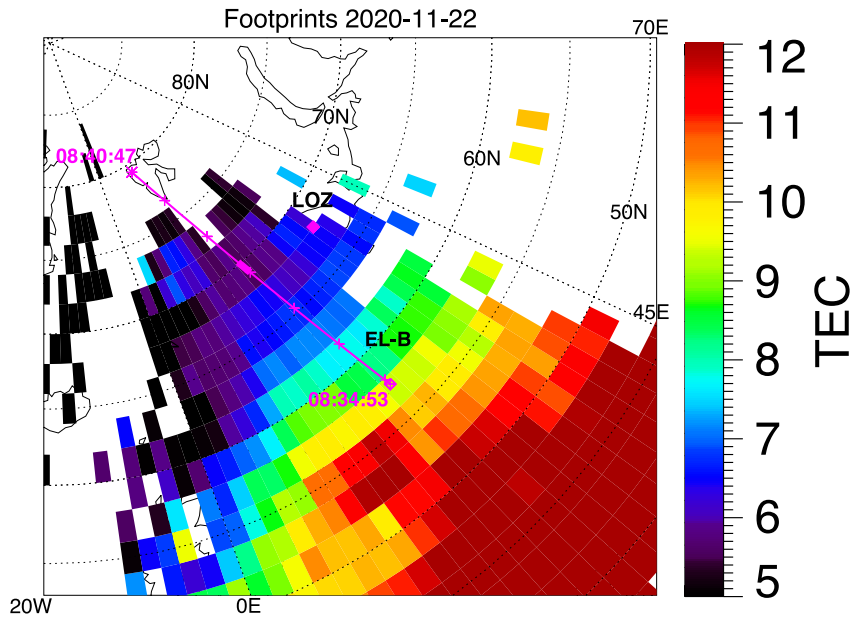

Figure 12. TEC map and the projected ELFIN orbit for the event from Figure 10. Diamonds and asterisks mark the start and end times of the trajectories; crosses are 1 min tickmarks; thick trace denotes times of relativistic electron precipitation identified from Figure 10c.

plasmapause (Dubyagin et al., 2011). This explains why the precipitation burst is projected to a region between the plasma sheet inner edge and the plasmapause.

The second mechanism is electron scattering by near-equatorial, very oblique whistler-mode waves (Artemyev et al., 2016; Lorentzen et al., 2001; Mourenas et al., 2014). These waves are indeed observed in the outer radiation belt (Agapitov et al., 2014; Cully et al., 2008; C. Cattell et al., 2008; C. A. Cattell et al., 2015). On the other hand, case studies of their role in electron precipitation do not show strong ~1 MeV precipitation (with precipitation-to-trapped flux ratio about one) (Gan et al., 2023; X.-J. Zhang, Artemyev, et al., 2022), that is, further investigations are needed to reveal the role of such very oblique waves in losses of relativistic electrons.

The dayside event shows a picture similar to night-side events: whistler-mode waves precipitate relativistic electrons at the outer edge of the inner magnetosphere (the inner edge of the dayside plasma sheet). The ground-based observations during this event show a very clear pattern of whistler-mode wave ducting. However, the relativistic electron precipitation burst is projected well outside the plasmapause. Therefore, other density gradients than those related to the plasmapause are needed to duct the whistler-mode waves. Although there are no plasma sheet injections on the day side, transient magnetopshere compressions can play a similar role in generating the whistler-mode waves and density perturbations (as needed for wave ducting). Such compressions can be produced by foreshock transients (Bentley et al., 2018; X. C. Shen et al., 2015; C.-P. Wang et al., 2017) and magnetopause dynamics (Agapitov et al., 2009; Hartinger et al., 2015; Hwang & Sibeck, 2016; Plaschke, 2016). Propagating into the inner magnetosphere as drifting mirror modes (Pokhotelov et al., 2001, 2003; Rae et al., 2007; Soto-Chavez et al., 2019) or standing Alfven waves (Wright & Elsden, 2020), compressional perturbations can modulate whistler-mode wave generation and cold plasma density structures (Li et al., 2011; Xia et al., 2020; X.-J. Zhang et al., 2019). Thus, such perturbations may provide sufficient conditions for whistler-mode wave ducting and relativistic electron precipitation.

To conclude, we have demonstrated relativistic electron precipitation events that cannot be explained by near-equatorial electron scattering due to field-aligned whistler-mode waves. Two possible mechanisms for these relativistic electron precipitation are wave ducting and propagation to the middle latitudes, and near-equatorial generation of very oblique waves. The ground-based measurements of whistler-mode waves support the wave ducting explanation. However, projection of ELFIN measurements to TEC maps reveals that if such wave ducting is associated with the relativistic precipitation events at ELFIN, it should occur well outside the plasmapause. Night-side injections and dayside transient compressions are potential candidate mechanisms to explain both

whistler-mode wave generation and the density gradients as needed for wave ducting. Further statistical investigation of relativistic electron precipitation observed by ELFIN together with TEC maps will reveal how often such precipitation events are observed outside the plasmapause and inside the inner edge of the plasma sheet. Note our data set includes only three events because the requirement of ground-based VLF measurements in conjunction with ELFIN observations is quite strict. However, these events are not unique from the point of view of ELFIN and equatorial measurements, and thus can be considered as representative of the subset of observed relativistic electron precipitation patterns. Note while we find ducted whistler mode waves as a reasonable explanation to explain the observed electron precipitation, our study falls short of categorically establishing ducting as the primary agent producing the precipitation.

Data Availability Statement

ELFIN data is available at https://data.elfin.ucla.edu/, THEMIS data is available at http://themis.ssl.berkeley.edu. MMS data is available at https://lasp.colorado.edu/mms/sdc/public/about/browse-wrapper/. GOES data is available at https://satdat.ngdc.noaa.gov/sem/goes/data/science/. POES data is available at https://www.ngdc.noaa.gov/stp/satellite/poes/index.html. Data access and processing was done using SPEDAS V3.1, see Angelopoulos et al. (2019). Data of ground-based VLF receivers is available at http://aurora.pgia.ru:8071/.

Acknowledgments

X.J.Z., A.V.A., and V.A. acknowledge support by NASA award NNX14AN68G, and NSF Grants AGS-1242918, AGS-2019950, and AGS-2329897. A.G.D. and Y.V.F. acknowledge support by the Russian Ministry of Education and Science under state task AAAA–A18–118012490100–7. Part of the research was performed at the Jet Propulsion Laboratory, California Institute of Technology, under a contract with National Aeronautics and Space Administration (80NM0018D0004). We are grateful to NASA's CubeSat Launch Initiative for ELFIN's successful launch in the desired orbits. We acknowledge early support of ELFIN project by the AFOSR, under its University Nanosat Program, UNP-8 project, contract FA9453-12-D-0285, and by the California Space Grant program. We acknowledge critical contributions of numerous volunteer ELFIN team student members.

References

Aa, E., Zou, S., Erickson, P. J., Zhang, S.-R., & Liu, S. (2020). Statistical analysis of the main ionospheric trough using swarm in situ measurements. *Journal of Geophysical Research: Space Physics*, *125*(3), e27583. https://doi.org/10.1029/2019JA027583

Agapitov, O. V., Artemyev, A., Krasnoselskikh, V., Khotyaintsev, Y. V., Mourenas, D., Breuillard, H., et al. (2013). Statistics of whistler mode waves in the outer radiation belt: Cluster STAFF-SA measurements. *Journal of Geophysical Research: Space Physics*, *118*(6), 3407–3420. https://doi.org/10.1002/jgra.50312

Agapitov, O. V., Artemyev, A., Mourenas, D., Krasnoselskikh, V., Bonnell, J., Le Contel, O., et al. (2014). The quasi-electrostatic mode of chorus waves and electron nonlinear acceleration. *Journal of Geophysical Research: Space Physics*, *119*(3), 1606–1626. https://doi.org/10.1002/2013JA019223

Agapitov, O. V., Glassmeier, K.-H., Plaschke, F., Auster, H.-U., Constantinescu, D., Angelopoulos, V., et al. (2009). Surface waves and field line resonances: A THEMIS case study. *Journal of Geophysical Research*, *114*(A1), A00C27. https://doi.org/10.1029/2008JA013553

Agapitov, O. V., Mourenas, D., Artemyev, A., Hospodarsky, G., & Bonnell, J. W. (2019). Time scales for electron quasi-linear diffusion by lower-band chorus waves: The effects of ω_{pe}/Ω_{ce} dependence on geomagnetic activity. *Geophysical Research Letters*, *46*(12), 6178–6187. https://doi.org/10.1029/2019GL083446

Agapitov, O. V., Mourenas, D., Artemyev, A. V., Mozer, F. S., Hospodarsky, G., Bonnell, J., & Krasnoselskikh, V. (2018). Synthetic empirical chorus wave model from combined Van Allen Probes and Cluster Statistics. *Journal of Geophysical Research: Space Physics*, *123*(1), 297–314. https://doi.org/10.1002/2017JA024843

An, X., Artemyev, A., Angelopoulos, V., Zhang, X., Mourenas, D., & Bortnik, J. (2022). Nonresonant scattering of relativistic electrons by electromagnetic ion cyclotron waves in Earth's radiation belts. *Physical Review Letters*, *129*(13), 135101. https://doi.org/10.1103/PhysRevLett.129.135101

Andronov, A. A., & Trakhtengerts, V. Y. (1964). Kinetic instability of the Earth's outer radiation belt. *Geomagnetism and Aeronomy*, *4*, 233–242.

Angelopoulos, V. (2008). The THEMIS mission. *Space Science Reviews*, *141*(1–4), 5–34. https://doi.org/10.1007/s11214-008-9336-1

Angelopoulos, V., Cruce, P., Drozdov, A., Grimes, E. W., Hatzigeorgiu, N., King, D. A., et al. (2019). The space physics environment data analysis System (SPEDAS). *Space Science Reviews*, *215*(1), 9. https://doi.org/10.1007/s11214-018-0576-4

Angelopoulos, V., Sibeck, D., Carlson, C. W., McFadden, J. P., Larson, D., Lin, R. P., et al. (2008). First results from the THEMIS mission. *Space Science Reviews*, *141*(1–4), 453–476. https://doi.org/10.1007/s11214-008-9378-4

Angelopoulos, V., Tsai, E., Bingley, L., Shaffer, C., Turner, D. L., Runov, A., et al. (2020). The ELFIN mission. *Space Science Reviews*, *216*(5), 103. https://doi.org/10.1007/s11214-020-00721-7

Angelopoulos, V., Zhang, X. J., Artemyev, A. V., Mourenas, D., Tsai, E., Wilkins, C., et al. (2022). Energetic electron precipitation driven by electromagnetic ion cyclotron waves from ELFIN's low altitude perspective. arXiv e-prints, arXiv:2211.15653. https://doi.org/10.48550/arXiv.2211.15653

Artemyev, A. V., Agapitov, O., Mourenas, D., Krasnoselskikh, V., Shastun, V., & Mozer, F. (2016). Oblique whistler-mode waves in the Earth's inner magnetosphere: Energy distribution, origins, and role in radiation belt dynamics. *Space Science Reviews*, *200*(1–4), 261–355. https://doi.org/10.1007/s11214-016-0252-5

Artemyev, A. V., Angelopoulos, V., Zhang, X. J., Runov, A., Petrukovich, A., Nakamura, R., et al. (2022). Thinning of the magnetotail current sheet inferred from low-altitude observations of energetic electrons. *Journal of Geophysical Research: Space Physics*, *127*(10), e2022JA030705. https://doi.org/10.1029/2022JA030705

Artemyev, A. V., Demekhov, A. G., Zhang, X. J., Angelopoulos, V., Mourenas, D., Fedorenko, Y. V., et al. (2021). Role of ducting in relativistic electron loss by whistler-mode wave scattering. *Journal of Geophysical Research: Space Physics*, *126*(11), e29851. https://doi.org/10.1029/2021JA029851

Artemyev, A. V., & Mourenas, D. (2020). On whistler mode wave relation to electron field-aligned plateau populations. *Journal of Geophysical Research: Space Physics*, *125*(3), e27735. https://doi.org/10.1029/2019JA027735

Artemyev, A. V., Mourenas, D., Agapitov, O. V., & Krasnoselskikh, V. V. (2013). Parametric validations of analytical lifetime estimates for radiation belt electron diffusion by whistler waves. *Annales Geophysicae*, *31*(4), 599–624. https://doi.org/10.5194/angeo-31-599-2013

Artemyev, A. V., Neishtadt, A. I., & Angelopoulos, V. (2022). On the role of whistler-mode waves in electron interaction with dipolarizing flux bundles. *Journal of Geophysical Research: Space Physics*, *127*(4), e30265. https://doi.org/10.1029/2022JA030265

Artemyev, A. V., Zhang, X. J., Zou, Y., Mourenas, D., Angelopoulos, V., Vainchtein, D., et al. (2022). On the nature of intense sub-relativistic electron precipitation. *Journal of Geophysical Research: Space Physics*, *127*(6), e30571. https://doi.org/10.1029/2022JA030571

Auster, H. U., Glassmeier, K. H., Magnes, W., Aydogar, O., Baumjohann, W., Constantinescu, D., et al. (2008). The THEMIS fluxgate magnetometer. *Space Science Reviews*, *141*(1–4), 235–264. https://doi.org/10.1007/s11214-008-9365-9

Belehaki, A., Jakowski, N., & Reinisch, B. W. (2004). Plasmaspheric electron content derived from GPS TEC and digisonde ionograms. *Advances in Space Research*, *33*(6), 833–837. https://doi.org/10.1016/j.asr.2003.07.008

Bell, T. F., Inan, U. S., Bortnik, J., & Scudder, J. D. (2002). The Landau damping of magnetospherically reflected whistlers within the plasmasphere. *Geophysical Research Letters*, *29*(15), 1733. https://doi.org/10.1029/2002GL014752

Bentley, S. N., Watt, C. E. J., Owens, M. J., & Rae, I. J. (2018). ULF wave activity in the magnetosphere: Resolving solar wind interdependencies to identify driving mechanisms. *Journal of Geophysical Research: Space Physics*, *123*(4), 2745–2771. https://doi.org/10.1002/2017JA024740

Bezděková, B., Němec, F., Manninen, J., Hospodarsky, G. B., Santolík, O., Kurth, W. S., & Hartley, D. P. (2020). Conjugate observations of quasiperiodic emissions by the Van Allen Probes spacecraft and ground-based station Kannuslehto. *Journal of Geophysical Research: Space Physics*, *125*(6), e27793. https://doi.org/10.1029/2020JA027793

Blake, J. B., Mauk, B. H., Baker, D. N., Carranza, P., Clemmons, J. H., Craft, J., et al. (2016). The fly's eye energetic particle spectrometer (FEEPS) sensors for the magnetospheric multiscale (MMS) mission. *Space Science Reviews*, *199*(1–4), 309–329. https://doi.org/10.1007/s11214-015-0163-x

Bortnik, J., Thorne, R. M., Meredith, N. P., & Santolik, O. (2007). Ray tracing of penetrating chorus and its implications for the radiation belts. *Geophysical Research Letters*, *34*(15), L15109. https://doi.org/10.1029/2007GL030040

Boudouridis, A., Rodriguez, J. V., Kress, B. T., Dichter, B. K., & Onsager, T. G. (2020). Development of a Bowtie inversion technique for real-time processing of the GOES-16/-17 SEISS MPS-HI electron channels. *Space Weather*, *18*(4), e02403. https://doi.org/10.1029/2019SW002403

Breneman, A. W., Crew, A., Sample, J., Klumpar, D., Johnson, A., Agapitov, O., et al. (2017). Observations directly linking relativistic electron microbursts to whistler mode chorus: Van Allen Probes and FIREBIRD II. *Geophysical Research Letters*, *44*(22), 11265–11272. https://doi.org/10.1002/2017GL075001

Breuillard, H., Le Contel, O., Retino, A., Chasapis, A., Chust, T., Mirioni, L., et al. (2016). Multispacecraft analysis of dipolarization fronts and associated whistler wave emissions using MMS data. *Geophysical Research Letters*, *43*(14), 7279–7286. https://doi.org/10.1002/2016GL069188

Burch, J. L., Moore, T. E., Torbert, R. B., & Giles, B. L. (2016). Magnetospheric multiscale overview and science objectives. *Space Science Reviews*, *199*(1–4), 5–21. https://doi.org/10.1007/s11214-015-0164-9

Capannolo, L., Li, W., Ma, Q., Qin, M., Shen, X. C., Angelopoulos, V., et al. (2023). Electron precipitation observed by elfin using proton precipitation as a proxy for electromagnetic ion cyclotron (emic) waves. *Geophysical Research Letters*, *50*(21). https://doi.org/10.1029/2023GL103519

Capannolo, L., Li, W., Spence, H., Johnson, A. T., Shumko, M., Sample, J., & Klumpar, D. (2021). Energetic electron precipitation observed by FIREBIRD II potentially driven by EMIC waves: Location, extent, and energy range from a multievent analysis. *Geophysical Research Letters*, *48*(5), e91564. https://doi.org/10.1029/2020GL091564

Carpenter, D., & Lemaire, J. (2004). The plasmasphere boundary layer. *Annales Geophysicae*, *22*(12), 4291–4298. https://doi.org/10.5194/angeo-22-4291-2004

Cattell, C., Wygant, J. R., Goetz, K., Kersten, K., Kellogg, P. J., von Rosenvinge, T., et al. (2008). Discovery of very large amplitude whistler-mode waves in Earth's radiation belts. *Geophysical Research Letters*, *35*(1), 1105. https://doi.org/10.1029/2007GL032009

Cattell, C. A., Breneman, A. W., Thaller, S. A., Wygant, J. R., Kletzing, C. A., & Kurth, W. S. (2015). Van Allen Probes observations of unusually low frequency whistler mode waves observed in association with moderate magnetic storms: Statistical study. *Geophysical Research Letters*, *42*(18), 7273–7281. https://doi.org/10.1002/2015GL065565

Chen, L., Breneman, A. W., Xia, Z., & Zhang, X.-j. (2020). Modeling of bouncing electron microbursts induced by ducted chorus waves. *Geophysical Research Letters*, *47*(17), e89400. https://doi.org/10.1029/2020GL089400

Chen, L., Thorne, R. M., Li, W., & Bortnik, J. (2013). Modeling the wave normal distribution of chorus waves. *Journal of Geophysical Research: Space Physics*, *118*(3), 1074–1088. https://doi.org/10.1029/2012JA018343

Chen, L., Zhang, X.-J., Artemyev, A., Angelopoulos, V., Tsai, E., Wilkins, C., & Horne, R. B. (2022). Ducted chorus waves cause sub-relativistic and relativistic electron microbursts. *Geophysical Research Letters*, *49*(5), e97559. https://doi.org/10.1029/2021GL097559

Chen, L., Zhang, X.-J., Artemyev, A., Zheng, L., Xia, Z., Breneman, A. W., & Horne, R. B. (2021). Electron microbursts induced by nonducted chorus waves. *Frontiers in Astronomy and Space Sciences*, *8*, 163. https://doi.org/10.3389/fspas.2021.745927

Chen, R., Gao, X., Lu, Q., Chen, L., Tsurutani, B. T., Li, W., & Wang, S. (2021). In situ observations of whistler mode chorus waves guided by density ducts. *Journal of Geophysical Research: Space Physics*, *126*(4), e28814. https://doi.org/10.1029/2020JA028814

Chen, R., Gao, X., Lu, Q., Tsurutani, B. T., & Wang, S. (2021). Observational evidence for whistler mode waves guided/ducted by the inner and outer edges of the plasmapause. *Geophysical Research Letters*, *48*(6), e92652. https://doi.org/10.1029/2021GL092652

Chen, Y., Reeves, G. D., Friedel, R. H. W., & Cunningham, G. S. (2014). Global time-dependent chorus maps from low-Earth-orbit electron precipitation and Van Allen Probes data. *Geophysical Research Letters*, *41*(3), 755–761. https://doi.org/10.1002/2013GL059181

Coster, A., Williams, J., Weatherwax, A., Rideout, W., & Herne, D. (2013). Accuracy of GPS total electron content: GPS receiver bias temperature dependence. *Radio Science*, *48*(2), 190–196. https://doi.org/10.1002/rds.20011

Cully, C. M., Bonnell, J. W., & Ergun, R. E. (2008). THEMIS observations of long-lived regions of large-amplitude whistler waves in the inner magnetosphere. *Geophysical Research Letters*, *35*, 17. https://doi.org/10.1029/2008GL033643

Demekhov, A. G., Manninen, J., Santolík, O., & Titova, E. E. (2017). Conjugate ground-spacecraft observations of VLF chorus elements. *Geophysical Research Letters*, *44*(23), 11735–11744. https://doi.org/10.1002/2017GL076139

Demekhov, A. G., Titova, E. E., Maninnen, J., Pasmanik, D. L., Lubchich, A. A., Santolík, O., et al. (2020). Localization of the source of quasiperiodic VLF emissions in the magnetosphere by using simultaneous ground and space observations: A case study. *Journal of Geophysical Research: Space Physics*, *125*(5), e27776. https://doi.org/10.1029/2020JA027776

Deng, X., Ashour-Abdalla, M., Zhou, M., Walker, R., El-Alaoui, M., Angelopoulos, V., et al. (2010). Wave and particle characteristics of earthward electron injections associated with dipolarization fronts. *Journal of Geophysical Research*, *115*(A9), A09225. https://doi.org/10.1029/2009JA015107

Denton, R. E., Takahashi, K., Galkin, I. A., Nsumei, P. A., Huang, X., Reinisch, B. W., et al. (2006). Distribution of density along magnetospheric field lines. *Journal of Geophysical Research*, *111*(A4), 4213. https://doi.org/10.1029/2005JA011414

Dichter, B. K., Galica, G. E., McGarity, J. O., Tsui, S., Golightly, M. J., Lopate, C., & Connell, J. J. (2015). Specification, design, and calibration of the space weather suite of instruments on the NOAA GOES-R Program spacecraft. *IEEE Transactions on Nuclear Science*, *62*(6), 2776–2783. https://doi.org/10.1109/TNS.2015.2477997

Dubyagin, S., Ganushkina, N. Y., & Sergeev, V. (2018). Formation of 30 KeV proton isotropic boundaries during geomagnetic storms. *Journal of Geophysical Research: Space Physics*, *123*(5), 3436–3459. https://doi.org/10.1002/2017JA024587

Dubyagin, S., Sergeev, V., Apatenkov, S., Angelopoulos, V., Runov, A., Nakamura, R., et al. (2011). Can flow bursts penetrate into the inner magnetosphere? *Geophysical Research Letters*, *38*(8), 8102. https://doi.org/10.1029/2011GL047016

Dubyagin, S., Sergeev, V. A., & Kubyshkina, M. V. (2002). On the remote sensing of plasma sheet from low-altitude spacecraft. *Journal of Atmospheric and Solar-Terrestrial Physics*, *64*(5–6), 567–572. https://doi.org/10.1016/S1364-6826(02)00014-7

Evans, D. S., & Greer, M. S. (2004). Polar orbiting environmental satellite space environment monitor-2: Instrument description and archive data documentation.

Fedorenko, Y., Tereshchenko, E., Pilgaev, S., Grigoryev, V., & Blagoveshchenskaya, N. (2014). Polarization of ELF waves generated during "beat-wave" heating experiment near cutoff frequency of the Earth-ionosphere waveguide. *Radio Science*, *49*(12), 1254–1264. https://doi.org/10.1002/2013RS005336

Fu, X., Cowee, M. M., Friedel, R. H., Funsten, H. O., Gary, S. P., Hospodarsky, G. B., et al. (2014). Whistler anisotropy instabilities as the source of banded chorus: Van Allen Probes observations and particle-in-cell simulations. *Journal of Geophysical Research: Space Physics*, *119*(10), 8288–8298. https://doi.org/10.1002/2014JA020364

Gan, L., Artemyev, A., Li, W., Zhang, X.-J., Ma, Q., Mourenas, D., et al. (2023). Bursty energetic electron precipitation by high-order resonance with very-oblique whistler-mode waves. *Geophysical Research Letters*, *50*(8), e2022GL101920. https://doi.org/10.1029/2022GL101920

Gkioulidou, M., Ohtani, S., Mitchell, D. G., Ukhorskiy, A. Y., Reeves, G. D., Turner, D. L., et al. (2015). Spatial structure and temporal evolution of energetic particle injections in the inner magnetosphere during the 14 july 2013 substorm event. *Journal of Geophysical Research: Space Physics*, *120*(3), 1924–1938. https://doi.org/10.1002/2014JA020872

Grach, V. S., Artemyev, A. V., Demekhov, A. G., Zhang, X.-J., Bortnik, J., Angelopoulos, V., et al. (2022). Relativistic electron precipitation by EMIC waves: Importance of nonlinear resonant effects. *Geophysical Research Letters*, *49*(17), e99994. https://doi.org/10.1029/2022GL099994

Hanzelka, M., & Santolík, O. (2019). Effects of ducting on whistler mode chorus or exohiss in the outer radiation belt. *Geophysical Research Letters*, *46*(11), 5735–5745. https://doi.org/10.1029/2019GL083115

Hartinger, M. D., Plaschke, F., Archer, M. O., Welling, D. T., Moldwin, M. B., & Ridley, A. (2015). The global structure and time evolution of dayside magnetopause surface eigenmodes. *Geophysical Research Letters*, *42*(8), 2594–2602. https://doi.org/10.1002/2015GL063623

Hartinger, M. D., Turner, D. L., Plaschke, F., Angelopoulos, V., & Singer, H. (2013). The role of transient ion foreshock phenomena in driving Pc5 ULF wave activity. *Journal of Geophysical Research: Space Physics*, *118*(1), 299–312. https://doi.org/10.1029/2012JA018349

Hartinger, M. D., Welling, D., Viall, N. M., Moldwin, M. B., & Ridley, A. (2014). The effect of magnetopause motion on fast mode resonance. *Journal of Geophysical Research: Space Physics*, *119*(10), 8212–8227. https://doi.org/10.1002/2014JA020401

Heilig, B., Stolle, C., Kervalishvili, G., Rauberg, J., Miyoshi, Y., Tsuchiya, F., et al. (2022). Relation of the plasmapause to the midlatitude ionospheric trough, the sub-auroral temperature enhancement and the distribution of small-scale field aligned currents as observed in the magnetosphere by THEMIS, RBSP, and arase, and in the topside ionosphere by swarm. *Journal of Geophysical Research: Space Physics*, *127*(3), e29646. https://doi.org/10.1029/2021JA029646

Heise, S., Jakowski, N., Wehrenpfennig, A., Reigber, C., & Lühr, H. (2002). Sounding of the topside ionosphere/plasmasphere based on GPS measurements from CHAMP: Initial results. *Geophysical Research Letters*, *29*(14), 1699. https://doi.org/10.1029/2002GL014738

Helliwell, R. A. (1965). *Whistlers and related ionospheric phenomena*. Stanford University Press.

Hikishima, M., Omura, Y., & Summers, D. (2010). Microburst precipitation of energetic electrons associated with chorus wave generation. *Geophysical Research Letters*, *37*(7), L07103. https://doi.org/10.1029/2010GL042678

Hosseini, P., Agapitov, O., Harid, V., & Gołkowski, M. (2021). Evidence of small scale plasma irregularity effects on whistler mode chorus propagation. *Geophysical Research Letters*, *48*(5), e92850. https://doi.org/10.1029/2021GL092850

Hwang, K. J., & Sibeck, D. G. (2016). Role of low-frequency boundary waves in the dynamics of the dayside magnetopause and the inner magnetosphere. In *Washington DC American Geophysical Union Geophysical Monograph Series* (Vol. 216, pp. 213–239). https://doi.org/10.1002/9781119055006.ch13

Imhof, W. L., Reagan, J. B., & Gaines, E. E. (1977). Fine-scale spatial structure in the pitch angle distributions of energetic particles near the midnight trapping boundary. *Journal of Geophysical Research*, *82*(32), 5215–5221. https://doi.org/10.1029/JA082i032p05215

Inan, U. S., & Bell, T. F. (1977). The plasmapause as a VLF wave guide. *Journal of Geophysical Research*, *82*(19), 2819–2827. https://doi.org/10.1029/JA082i019p02819

Karpman, V. I., & Kaufman, R. N. (1982). Whistler wave propagation in density ducts. *Journal of Plasma Physics*, *27*(2), 225–238. https://doi.org/10.1017/S0022377800026556

Ke, Y., Chen, L., Gao, X., Lu, Q., Wang, X., Chen, R., et al. (2021). Whistler mode waves trapped by density irregularities in the Earth's magnetosphere. *Geophysical Research Letters*, *48*(7), e92305. https://doi.org/10.1029/2020GL092305

Kennel, C. F. (1969). Consequences of a magnetospheric plasma. *Reviews of Geophysics and Space Physics*, *7*(1–2), 379–419. https://doi.org/10.1029/RG007i001p00379

Kennel, C. F., & Engelmann, F. (1966). Velocity space diffusion from weak plasma turbulence in a magnetic field. *Physics of Fluids*, *9*(12), 2377–2388. https://doi.org/10.1063/1.1761629

Kennel, C. F., & Petschek, H. E. (1966). Limit on stably trapped particle Fluxes. *Journal of Geophysical Research*, *71*, 1–28. https://doi.org/10.1029/jz071i001p00001

Laird, M. J., & Nunn, D. (1975). Full-wave VLF modes in a cylindrically symmetric enhancement of plasma density. *Planatary Space Science*, *23*(12), 1649–1657. https://doi.org/10.1016/0032-0633(75)90092-6

Le Contel, O., Roux, A., Jacquey, C., Robert, P., Berthomier, M., Chust, T., et al. (2009). Quasi-parallel whistler mode waves observed by THEMIS during near-earth dipolarizations. *Annales Geophysicae*, *27*(6), 2259–2275. https://doi.org/10.5194/angeo-27-2259-2009

Lee, H. B., Jee, G., Kim, Y. H., & Shim, J. S. (2013). Characteristics of global plasmaspheric TEC in comparison with the ionosphere simultaneously observed by Jason-1 satellite. *Journal of Geophysical Research: Space Physics*, *118*(2), 935–946. https://doi.org/10.1002/jgra.50130

Li, W., Bortnik, J., Thorne, R. M., Nishimura, Y., Angelopoulos, V., & Chen, L. (2011). Modulation of whistler mode chorus waves: 2. Role of density variations. *Journal of Geophysical Research*, *116*(A6), A06206. https://doi.org/10.1029/2010JA016313

Li, W., & Hudson, M. K. (2019). Earth's Van Allen radiation belts: From discovery to the Van Allen Probes era. *Journal of Geophysical Research: Space Physics*, *124*(11), 8319–8351. https://doi.org/10.1029/2018JA025940

Li, W., Ma, Q., Thorne, R. M., Bortnik, J., Kletzing, C. A., Kurth, W. S., et al. (2015). Statistical properties of plasmaspheric hiss derived from Van Allen Probes data and their effects on radiation belt electron dynamics. *Journal of Geophysical Research: Space Physics*, *120*(5), 3393–3405. https://doi.org/10.1002/2015JA021048

Li, W., Mourenas, D., Artemyev, A., Agapitov, O., Bortnik, J., Albert, J., et al. (2014). Evidence of stronger pitch angle scattering loss caused by oblique whistler-mode waves as compared with quasi-parallel waves. *Geophysical Research Letters*, *41*(17), 6063–6070. https://doi.org/10.1002/2014GL061260

Li, W., Ni, B., Thorne, R. M., Bortnik, J., Green, J. C., Kletzing, C. A., et al. (2013). Constructing the global distribution of chorus wave intensity using measurements of electrons by the POES satellites and waves by the Van Allen Probes. *Geophysical Research Letters*, *40*(17), 4526–4532. https://doi.org/10.1002/grl.50920

Li, W., Thorne, R. M., Bortnik, J., Baker, D. N., Reeves, G. D., Kanekal, S. G., et al. (2015). Solar wind conditions leading to efficient radiation belt electron acceleration: A superposed epoch analysis. *Geophysical Research Letters*, *42*(17), 6906–6915. https://doi.org/10.1002/2015GL065342

Liu, J., Angelopoulos, V., Zhang, X.-J., Turner, D. L., Gabrielse, C., Runov, A., et al. (2016). Dipolarizing flux bundles in the cis-geosynchronous magnetosphere: Relationship between electric fields and energetic particle injections. *Journal of Geophysical Research: Space Physics*, *121*(2), 1362–1376. https://doi.org/10.1002/2015JA021691

Lorentzen, K. R., Blake, J. B., Inan, U. S., & Bortnik, J. (2001). Observations of relativistic electron microbursts in association with VLF chorus. *Journal of Geophysical Research*, *106*(A4), 6017–6028. https://doi.org/10.1029/2000JA003018

Lyons, L. R., Gallardo-Lacourt, B., Zou, S., Weygand, J. M., Nishimura, Y., Li, W., et al. (2016). The 17 March 2013 storm: Synergy of observations related to electric field modes and their ionospheric and magnetospheric Effects. *Journal of Geophysical Research: Space Physics*, *121*(11), 10880–10897. https://doi.org/10.1002/2016JA023237

Lyons, L. R., Thorne, R. M., & Kennel, C. F. (1972). Pitch-angle diffusion of radiation belt electrons within the plasmasphere. *Journal of Geophysical Research*, *77*(19), 3455–3474. https://doi.org/10.1029/JA077i019p03455

Ma, Q., Mourenas, D., Li, W., Artemyev, A., & Thorne, R. M. (2017). VLF waves from ground-based transmitters observed by the Van Allen Probes: Statistical model and effects on plasmaspheric electrons. *Geophysical Research Letters*, *44*(13), 6483–6491. https://doi.org/10.1002/2017GL073885

Malaspina, D. M., Jaynes, A. N., Hospodarsky, G., Bortnik, J., Ergun, R. E., & Wygant, J. (2017). Statistical properties of low-frequency plasmaspheric hiss. *Journal of Geophysical Research: Space Physics*, *122*(8), 8340–8352. https://doi.org/10.1002/2017JA024328

Manninen, J., Kleimenova, N. G., Kozyreva, O. V., Bespalov, P. A., & Kozlovsky, A. E. (2013). Non-typical ground-based quasi-periodic VLF emissions observed at $L\sum$5.3 under quiet geomagnetic conditions at night. *Journal of Atmospheric and Solar-Terrestrial Physics*, *99*, 123–128. https://doi.org/10.1016/j.jastp.2012.05.007

Martinez-Calderon, C., Katoh, Y., Manninen, J., Kasahara, Y., Matsuda, S., Kumamoto, A., et al. (2020). Conjugate observations of dayside and nightside VLF chorus and QP emissions between arase (ERG) and Kannuslehto, Finland. *Journal of Geophysical Research: Space Physics*, *125*(1), e26663. https://doi.org/10.1029/2019JA026663

Martinez-Calderon, C., Shiokawa, K., Miyoshi, Y., Keika, K., Ozaki, M., Schofield, I., et al. (2016). ELF/VLF wave propagation at subauroral latitudes: Conjugate observation between the ground and Van Allen Probes A. *Journal of Geophysical Research: Space Physics*, *121*(6), 5384–5393. https://doi.org/10.1002/2015JA022264

Martinez-Calderon, C., Shiokawa, K., Miyoshi, Y., Ozaki, M., Schofield, I., & Connors, M. (2015). Statistical study of ELF/VLF emissions at subauroral latitudes in Athabasca, Canada. *Journal of Geophysical Research: Space Physics*, *120*(10), 8455–8469. https://doi.org/10.1002/2015JA021347

Maxworth, A. S., & Golkowski, M. (2017). Magnetospheric whistler mode ray tracing in a warm background plasma with finite electron and ion temperature. *Journal of Geophysical Research: Space Physics*, *122*(7), 7323–7335. https://doi.org/10.1002/2016JA023546

McFadden, J. P., Carlson, C. W., Larson, D., Ludlam, M., Abiad, R., Elliott, B., et al. (2008). The THEMIS ESA plasma instrument and in-flight calibration. *Space Science Reviews*, *141*(1–4), 277–302. https://doi.org/10.1007/s11214-008-9440-2

Meredith, N. P., Horne, R. B., Clilverd, M. A., & Ross, J. P. J. (2019). An investigation of VLF transmitter wave power in the inner radiation belt and slot region. *Journal of Geophysical Research: Space Physics*, *124*(7), 5246–5259. https://doi.org/10.1029/2019JA026715

Meredith, N. P., Horne, R. B., Sicard-Piet, A., Boscher, D., Yearby, K. H., Li, W., & Thorne, R. M. (2012). Global model of lower band and upper band chorus from multiple satellite observations. *Journal of Geophysical Research*, *117*(A10), 10225. https://doi.org/10.1029/2012JA017978

Millan, R. M., & Thorne, R. M. (2007). Review of radiation belt relativistic electron losses. *Journal of Atmospheric and Solar-Terrestrial Physics*, *69*(3), 362–377. https://doi.org/10.1016/j.jastp.2006.06.019

Miyoshi, Y., Hosokawa, S., Kurita, S.-I., Oyama, Y., Ogawa, S., Saito, I., et al. (2021). Penetration of MeV electrons into the mesosphere accompanying pulsating aurorae. *Scientific Reports*, *11*(1), 13724. https://doi.org/10.1038/s41598-021-92611-3

Miyoshi, Y., Saito, S., Kurita, S., Asamura, K., Hosokawa, K., Sakanoi, T., et al. (2020). Relativistic electron microbursts as high-energy tail of pulsating aurora electrons. *Geophysical Research Letters*, *47*(21), e90360. https://doi.org/10.1029/2020GL090360

Motoba, T., Ohtani, S., Gkioulidou, M., Mitchell, D. G., Ukhorskiy, A. Y., Takahashi, K., et al. (2020). Pitch angle dependence of electron and ion flux changes during local magnetic dipolarization inside geosynchronous orbit. *Journal of Geophysical Research: Space Physics*, *125*(2), e27543. https://doi.org/10.1029/2019JA027543

Mourenas, D., Artemyev, A. V., Agapitov, O. V., & Krasnoselskikh, V. (2014). Consequences of geomagnetic activity on energization and loss of radiation belt electrons by oblique chorus waves. *Journal of Geophysical Research: Space Physics*, *119*(4), 2775–2796. https://doi.org/10.1002/2013JA019674

Mourenas, D., Artemyev, A. V., Agapitov, O. V., Krasnoselskikh, V., & Mozer, F. S. (2015). Very oblique whistler generation by low-energy electron streams. *Journal of Geophysical Research: Space Physics*, *120*(5), 3665–3683. https://doi.org/10.1002/2015JA021135

Mourenas, D., Artemyev, A. V., Zhang, X. J., Angelopoulos, V., Tsai, E., & Wilkins, C. (2021). Electron lifetimes and diffusion rates inferred from ELFIN measurements at low altitude: First results. *Journal of Geophysical Research: Space Physics*, *126*(11), e29757. https://doi.org/10.1029/2021JA029757

Mozer, F. S., Agapitov, O. V., Blake, J. B., & Vasko, I. Y. (2018). Simultaneous observations of lower band chorus emissions at the equator and microburst precipitating electrons in the ionosphere. *Geophysical Research Letters*, *45*(2), 511–516. https://doi.org/10.1002/2017GL076120

O'Brien, T. P., Looper, M. D., & Blake, J. B. (2004). Quantification of relativistic electron microburst losses during the GEM storms. *Geophysical Research Letters*, *31*(4), L04802. https://doi.org/10.1029/2003GL018621

Pasmanik, D. L., & Trakhtengerts, V. Y. (2005). Dispersion properties of ducted whistlers, generated by lightning discharge. *Annales Geophysicae*, *23*(4), 1433–1439. https://doi.org/10.5194/angeo-23-1433-2005

Plaschke, F. (2016). ULF waves at the magnetopause. In *Washington DC American Geophysical Union Geophysical Monograph Series* (Vol. 216, pp. 193–212). https://doi.org/10.1002/9781119055006.ch12

Pokhotelov, O. A., Balikhin, M. A., Treumann, R. A., & Pavlenko, V. P. (2001). Drift mirror instability revisited: 1. Cold electron temperature limit. *Journal of Geophysical Research*, *106*(A5), 8455–8464. https://doi.org/10.1029/2000JA000069

Pokhotelov, O. A., Sandberg, I., Sagdeev, R. Z., Treumann, R. A., Onishchenko, O. G., Balikhin, M. A., & Pavlenko, V. P. (2003). Slow drift mirror modes in finite electron-temperature plasma: Hydrodynamic and kinetic drift mirror instabilities. *Journal of Geophysical Research*, *108*(A3), 1098. https://doi.org/10.1029/2002JA009651

Rae, I. J., Mann, I. R., Watt, C. E. J., Kistler, L. M., & Baumjohann, W. (2007). Equator-S observations of drift mirror mode waves in the dawnside magnetosphere. *Journal of Geophysical Research*, *112*(A11), A11203. https://doi.org/10.1029/2006JA012064

Rideout, W., & Coster, A. (2006). Automated GPS processing for global total electron content data. *GPS Solutions*, *10*(3), 219–228. https://doi.org/10.1007/s10291-006-0029-5

Runov, A., Angelopoulos, V., Gabrielse, C., Liu, J., Turner, D. L., & Zhou, X.-Z. (2015). Average thermodynamic and spectral properties of plasma in and around dipolarizing flux bundles. *Journal of Geophysical Research: Space Physics*, *120*(6), 4369–4383. https://doi.org/10.1002/2015JA021166

Runov, A., Angelopoulos, V., Sitnov, M. I., Sergeev, V. A., Bonnell, J., McFadden, J. P., et al. (2009). THEMIS observations of an earthward-propagating dipolarization front. *Geophysical Research Letters*, *36*(14), L14106. https://doi.org/10.1029/2009GL038980

Runov, A., Angelopoulos, V., Zhou, X.-Z., Zhang, X.-J., Li, S., Plaschke, F., & Bonnell, J. (2011). A THEMIS multicase study of dipolarization fronts in the magnetotail plasma sheet. *Journal of Geophysical Research*, *116*(A5), 5216. https://doi.org/10.1029/2010JA016316

Russell, C. T., Anderson, B. J., Baumjohann, W., Bromund, K. R., Dearborn, D., Fischer, D., et al. (2016). The magnetospheric multiscale magnetometers. *Space Science Reviews*, *199*(1–4), 189–256. https://doi.org/10.1007/s11214-014-0057-3

Sergeev, V. A., Angelopoulos, V., Apatenkov, S., Bonnell, J., Ergun, R., Nakamura, R., et al. (2009). Kinetic structure of the sharp injection/dipolarization front in the flow-braking region. *Geophysical Research Letters*, *36*(21), 21105. https://doi.org/10.1029/2009GL040658

Sergeev, V. A., Angelopoulos, V., Carlson, C., & Sutcliffe, P. (1998). Current sheet measurements within a flapping plasma sheet. *Journal of Geophysical Research*, *103*(A5), 9177–9188. https://doi.org/10.1029/97JA02093

Sergeev, V. A., Angelopoulos, V., Kubyshkina, M., Donovan, E., Zhou, X.-Z., Runov, A., et al. (2011). Substorm growth and expansion onset as observed with ideal ground-spacecraft THEMIS coverage. *Journal of Geophysical Research*, *116*(A5), A00I26. https://doi.org/10.1029/2010JA015689

Sergeev, V. A., Chernyaev, I. A., Angelopoulos, V., Runov, A. V., & Nakamura, R. (2014). Stopping flow bursts and their role in the generation of the substorm current wedge. *Geophysical Research Letters*, *41*(4), 1106–1112. https://doi.org/10.1002/2014GL059309

Sergeev, V. A., Kubyshkina, M. V., Semenov, V., Artemyev, A., Angelopoulos, V., & Runov, A. (2023). Unusual magnetospheric dynamics during intense substorm initiated by strong magnetospheric compression. *Journal of Geophysical Research: Space Physics*, *128*(11). https://doi.org/10.1029/2023JA031536

Sergeev, V. A., Nishimura, Y., Kubyshkina, M., Angelopoulos, V., Nakamura, R., & Singer, H. (2012). Magnetospheric location of the equatorward prebreakup arc. *Journal of Geophysical Research*, *117*(A1), A01212. https://doi.org/10.1029/2011JA017154

Sheeley, B. W., Moldwin, M. B., Rassoul, H. K., & Anderson, R. R. (2001). An empirical plasmasphere and trough density model: CRRES observations. *Journal of Geophysical Research*, *106*(A11), 25631–25642. https://doi.org/10.1029/2000JA000286

Shen, X. C., Zong, Q. G., Shi, Q. Q., Tian, A. M., Sun, W. J., Wang, Y. F., et al. (2015). Magnetospheric ULF waves with increasing amplitude related to solar wind dynamic pressure changes: The Time History of Events and Macroscale Interactions during Substorms (THEMIS) observations. *Journal of Geophysical Research: Space Physics*, *120*(9), 7179–7190. https://doi.org/10.1002/2014JA020913

Shen, Y., Chen, L., Zhang, X.-J., Artemyev, A., Angelopoulos, V., Cully, C. M., et al. (2021). Conjugate observation of magnetospheric chorus propagating to the ionosphere by ducting. *Geophysical Research Letters*, *48*(23), e95933. https://doi.org/10.1029/2021GL095933

Shi, X., Zhang, X., Artemyev, A. V., Angelopoulos, V., Hartinger, M. D., Tsai, E., & Wilkins, C. (2022a). On the role of ulf waves in the spatial and temporal periodicity of energetic electron precipitation. *Earth and Space Science Open Archive*, *20*. https://doi.org/10.1002/essoar.10512214.1

Shi, X., Zhang, X.-J., Artemyev, A., Angelopoulos, V., Hartinger, M. D., Tsai, E., & Wilkins, C. (2022b). On the role of ULF waves in the spatial and temporal periodicity of energetic electron precipitation. *Journal of Geophysical Research: Space Physics*, *127*(12), e2022JA030932. https://doi.org/10.1029/2022JA030932

Shinbori, A., Otsuka, Y., Tsugawa, T., Nishioka, M., Kumamoto, A., Tsuchiya, F., et al. (2021). Relationship between the locations of the midlatitude trough and plasmapause using GNSS TEC and arase satellite observation data. *Journal of Geophysical Research: Space Physics*, *126*(5), e28943. https://doi.org/10.1029/2020JA028943

Shiokawa, K., Katoh, Y., Hamaguchi, Y., Yamamoto, Y., Adachi, T., Ozaki, M., et al. (2017). Ground-based instruments of the PWING project to investigate dynamics of the inner magnetosphere at subauroral latitudes as a part of the ERG-ground coordinated observation network. *Earth Planets and Space*, *69*(1), 160. https://doi.org/10.1186/s40623-017-0745-9

Shklyar, D. R., Chum, J., & Jiřícek, F. (2004). Characteristic properties of Nu whistlers as inferred from observations and numerical modelling. *Annales Geophysicae*, *22*(10), 3589–3606. https://doi.org/10.5194/angeo-22-3589-2004

Shue, J.-H., Chao, J. K., Fu, H. C., Russell, C. T., Song, P., Khurana, K. K., & Singer, H. J. (1997). A new functional form to study the solar wind control of the magnetopause size and shape. *Journal of Geophysical Research*, *102*(A5), 9497–9512. https://doi.org/10.1029/97JA00196

Shumko, M., Gallardo-Lacourt, B., Halford, A. J., Liang, J., Blum, L. W., Donovan, E., et al. (2021). A strong correlation between relativistic electron microbursts and patchy aurora. *Geophysical Research Letters*, *48*(18), e94696. https://doi.org/10.1029/2021GL094696

Shumko, M., Turner, D. L., O'Brien, T. P., Claudepierre, S. G., Sample, J., Hartley, D. P., et al. (2018). Evidence of microbursts observed near the equatorial plane in the outer Van Allen radiation belt. *Geophysical Research Letters*, *45*(16), 8044–8053. https://doi.org/10.1029/2018GL078451

Singer, H. J., Matheson, L., Grubb, R., Newman, A., & Bouwer, S. D. (1996). Monitoring space weather with the goes magnetometers in goes-8 and beyond (Tech. Rep. No. 2812). In E. R. Washwell (Ed.).*SPIE Conference Proceedings*.

Sitnov, M. I., Stephens, G. K., Tsyganenko, N. A., Miyashita, Y., Merkin, V. G., Motoba, T., et al. (2019). Signatures of nonideal plasma evolution during substorms obtained by mining multimission magnetometer data. *Journal of Geophysical Research: Space Physics*, *124*(11), 8427–8456. https://doi.org/10.1029/2019JA027037

Soto-Chavez, A. R., Lanzerotti, L. J., Manweiler, J. W., Gerrard, A., Cohen, R., Xia, Z., et al. (2019). Observational evidence of the drift-mirror plasma instability in Earth's inner magnetosphere. *Physics of Plasmas*, *26*(4), 042110. https://doi.org/10.1063/1.5083629

Stephens, G. K., & Sitnov, M. I. (2021). Concurrent empirical magnetic reconstruction of storm and substorm spatial scales using data mining and virtual spacecraft. *Frontiers in Physics*, *9*, 210. https://doi.org/10.3389/fphy.2021.653111

Streltsov, A. V., & Bengtson, M. T. (2020). Observations and modeling of whistler mode waves in the magnetospheric density ducts. *Journal of Geophysical Research: Space Physics*, *125*(10), e28398. https://doi.org/10.1029/2020JA028398

Streltsov, A. V., & Goyal, R. (2021). Whistlers in micro ducts. *Journal of Geophysical Research: Space Physics*, *126*(11), e29868. https://doi.org/10.1029/2021JA029868

Summers, D., Ni, B., & Meredith, N. P. (2007a). Timescales for radiation belt electron acceleration and loss due to resonant wave-particle interactions: 1. Theory. *Journal of Geophysical Research*, *112*(A4), 4206. https://doi.org/10.1029/2006JA011801

Summers, D., Ni, B., & Meredith, N. P. (2007b). Timescales for radiation belt electron acceleration and loss due to resonant wave-particle interactions: 2. Evaluation for VLF chorus, ELF hiss, and electromagnetic ion cyclotron waves. *Journal of Geophysical Research*, *112*(A4), 4207. https://doi.org/10.1029/2006JA011993

Summers, D., & Thorne, R. M. (2003). Relativistic electron pitch-angle scattering by electromagnetic ion cyclotron waves during geomagnetic storms. *Journal of Geophysical Research*, *108*(A4), 1143. https://doi.org/10.1029/2002JA009489

Tao, X., Thorne, R. M., Li, W., Ni, B., Meredith, N. P., & Horne, R. B. (2011). Evolution of electron pitch angle distributions following injection from the plasma sheet. *Journal of Geophysical Research*, *116*(A4), A04229. https://doi.org/10.1029/2010JA016245

Thorne, R. M., Bortnik, J., Li, W., & Ma, Q. (2021). Wave–particle interactions in the Earth's magnetosphere. In *Magnetospheres in the solar system* (pp. 93–108). American Geophysical Union (AGU). https://doi.org/10.1002/9781119815624.ch6

Thorne, R. M., O'Brien, T. P., Shprits, Y. Y., Summers, D., & Horne, R. B. (2005). Timescale for MeV electron microburst loss during geomagnetic storms. *Journal of Geophysical Research*, *110*(A9), 9202. https://doi.org/10.1029/2004JA010882

Titova, E. E., Demekhov, A. G., Manninen, J., Pasmanik, D. L., & Larchenko, A. V. (2017). Localization of the sources of narrow-band noise VLF emissions in the range 4-10 kHz from simultaneous ground-based and Van Allen Probes satellite observations. *Geomagnetism and Aeronomy*, *57*(6), 706–718. https://doi.org/10.1134/S0016793217060135

Titova, E. E., Kozelov, B. V., Demekhov, A. G., Manninen, J., Santolik, O., Kletzing, C. A., & Reeves, G. (2015). Identification of the source of quasi-periodic VLF emissions using ground-based and Van Allen Probes satellite observations. *Geophysical Research Letters*, *42*(15), 6137–6145. https://doi.org/10.1002/2015GL064911

Tsai, E., Artemyev, A., Angelopoulos, V., & Zhang, X.-J. (2023). Investigating whistler-mode wave intensity along field lines using electron precipitation measurements. *Journal of Geophysical Research: Space Physics*, *128*(8), e2023JA031578. https://doi.org/10.1029/2023JA031578

Tsai, E., Artemyev, A., Zhang, X.-J., & Angelopoulos, V. (2022). Relativistic electron precipitation driven by nonlinear resonance with whistler-mode waves. *Journal of Geophysical Research: Space Physics*, *127*(5), e30338. https://doi.org/10.1029/2022JA030338

Tsurutani, B. T., Lakhina, G. S., & Verkhoglyadova, O. P. (2013). Energetic electron (>10 keV) microburst precipitation, 5-15 s X-ray pulsations, chorus, and wave-particle interactions: A review. *Journal of Geophysical Research: Space Physics*, *118*(5), 2296–2312. https://doi.org/10.1002/jgra.50264

Tsyganenko, N. A. (1989). A magnetospheric magnetic field model with a warped tail current sheet. *Planatary Space Science*, *37*(1), 5–20. https://doi.org/10.1016/0032-0633(89)90066-4

Tsyganenko, N. A. (1995). Modeling the Earth's magnetospheric magnetic field confined within a realistic magnetopause. *Journal of Geophysical Research*, *100*(A4), 5599–5612. https://doi.org/10.1029/94JA03193

Tsyganenko, N. A., & Sitnov, M. I. (2005). Modeling the dynamics of the inner magnetosphere during strong geomagnetic storms. *Journal of Geophysical Research*, *110*(A3), A03208. https://doi.org/10.1029/2004JA010798

Turner, D. L., Fennell, J. F., Blake, J. B., Claudepierre, S. G., Clemmons, J. H., Jaynes, A. N., et al. (2017). Multipoint observations of energetic particle injections and substorm activity during a conjunction between magnetospheric multiscale (MMS) and Van Allen Probes. *Journal of Geophysical Research: Space Physics*, *122*(11), 11481–11504. https://doi.org/10.1002/2017JA024554

Ukhorskiy, A. Y., Sorathia, K. A., Merkin, V. G., Crabtree, C., Fletcher, A. C., Malaspina, D. M., & Schwartz, S. J. (2022). Cross-scale energy cascade powered by magnetospheric convection. *Scientific Reports*, *12*(1), 4446. https://doi.org/10.1038/s41598-022-08038-x

Vasko, I. Y., Agapitov, O. V., Mozer, F. S., Bonnell, J. W., Artemyev, A. V., Krasnoselskikh, V. V., et al. (2017). Electron-acoustic solitons and double layers in the inner magnetosphere. *Geophysical Research Letters*, *44*(10), 4575–4583. https://doi.org/10.1002/2017GL074026

Vierinen, J., Coster, A. J., Rideout, W. C., Erickson, P. J., & Norberg, J. (2015). Statistical framework for estimating GNSS bias. *Atmospheric Measurement Techniques Discussions*, *8*(9), 9373–9398. https://doi.org/10.5194/amtd-8-9373-2015

Vo, H. B., & Foster, J. C. (2001). A quantitative study of ionospheric density gradients at midlatitudes. *Journal of Geophysical Research*, *106*(A10), 21555–21564. https://doi.org/10.1029/2000JA000397

Wang, C.-P., Thorne, R., Liu, T. Z., Hartinger, M. D., Nagai, T., Angelopoulos, V., et al. (2017). A multispacecraft event study of Pc5 ultralow-frequency waves in the magnetosphere and their external drivers. *Journal of Geophysical Research: Space Physics*, *122*(5), 5132–5147. https://doi.org/10.1002/2016JA023610

Wang, D., & Shprits, Y. Y. (2019). On how high-latitude chorus waves tip the balance between acceleration and loss of relativistic electrons. *Geophysical Research Letters*, *46*(14), 7945–7954. https://doi.org/10.1029/2019GL082681

Watt, C. E. J., Degeling, A. W., & Rankin, R. (2013). Constructing the frequency and wave normal distribution of whistler-mode wave power. *Journal of Geophysical Research: Space Physics*, *118*(5), 1984–1991. https://doi.org/10.1002/jgra.50231

Weygand, J. M., Zhelavskaya, I., & Shprits, Y. (2021). A comparison of the location of the mid latitude trough and plasmapause boundary. *Journal of Geophysical Research: Space Physics*, *126*(4), e28213. https://doi.org/10.1029/2020JA028213

Wilkins, C., Angelopoulos, V., Runov, A., Artemyev, A., Zhang, X. J., Liu, J., & Tsai, E. (2023). Statistical characteristics of the electron isotropy boundary. *Journal of Geophysical Research: Space Physics*, *128*(10), e2023JA031774. https://doi.org/10.1029/2023JA031774

Williams, D. D., & Streltsov, A. V. (2021). Determining parameters of whistler waves trapped in high-density ducts. *Journal of Geophysical Research: Space Physics*, *126*(12), e29228. https://doi.org/10.1029/2021JA029228

Woodroffe, J. R., & Streltsov, A. V. (2013). Whistler propagation in the plasmapause. *Journal of Geophysical Research: Space Physics*, *118*(2), 716–723. https://doi.org/10.1002/jgra.50135

Wright, A. N., & Elsden, T. (2020). Simulations of mhd wave propagation and coupling in a 3-d magnetosphere. *Journal of Geophysical Research: Space Physics*, *125*(2), e2019JA027589. https://doi.org/10.1029/2019JA027589

Wu, D. J., Chao, J. K., & Lepping, R. P. (2000). Interaction between an interplanetary magnetic cloud and the Earth's magnetosphere: Motions of the bow shock. *Journal of Geophysical Research*, *105*(A6), 12627–12638. https://doi.org/10.1029/1999JA000265

Xia, Z., Chen, L., & Li, W. (2020). Statistical study of chorus modulations by background magnetic field and plasma density. *Geophysical Research Letters*, *47*(22), e89344. https://doi.org/10.1029/2020GL089344

Yizengaw, E., & Moldwin, M. B. (2005). The altitude extension of the mid-latitude trough and its correlation with plasmapause position. *Geophysical Research Letters*, *32*(9), L09105. https://doi.org/10.1029/2005GL022854

Zhang, X., Angelopoulos, V., Artemyev, A. V., & Liu, J. (2018). Whistler and electron firehose instability control of electron distributions in and around dipolarizing flux bundles. *Geophysical Research Letters*, *45*(18), 9380–9389. https://doi.org/10.1029/2018GL079613

Zhang, X.-J., Angelopoulos, V., Artemyev, A., Mourenas, D., Agapitov, O., Tsai, E., & Wilkins, C. (2023). Temporal scales of electron precipitation driven by whistler-mode waves. *Journal of Geophysical Research: Space Physics*, *128*(1), e2022JA031087. https://doi.org/10.1029/2022JA031087

Zhang, X. J., Angelopoulos, V., Artemyev, A. V., Hartinger, M. D., & Bortnik, J. (2020). Modulation of whistler waves by ultra-low-frequency perturbations: The importance of magnetopause location. *Journal of Geophysical Research: Space Physics*, *125*(10), e28334. https://doi.org/10.1029/2020JA028334

Zhang, X.-J., Angelopoulos, V., Mourenas, D., Artemyev, A., Tsai, E., & Wilkins, C. (2022). Characteristics of electron microburst precipitation based on high-resolution ELFIN measurements. *Journal of Geophysical Research: Space Physics*, *127*(5), e30509. https://doi.org/10.1029/2022JA030509

Zhang, X.-J., Artemyev, A., Angelopoulos, V., Tsai, E., Wilkins, C., Kasahara, S., et al. (2022). Superfast precipitation of energetic electrons in the radiation belts of the Earth. *Nature Communications*, *13*(1), 1611. https://doi.org/10.1038/s41467-022-29291-8

Zhang, X.-J., Chen, L., Artemyev, A. V., Angelopoulos, V., & Liu, X. (2019). Periodic excitation of chorus and ECH waves modulated by ultralow frequency compressions. *Journal of Geophysical Research: Space Physics*, *124*(11), 8535–8550. https://doi.org/10.1029/2019JA027201

Zhang, Z., Chen, L., Li, X., Xia, Z., Heelis, R. A., & Horne, R. B. (2018). Observed propagation route of VLF transmitter signals in the magnetosphere. *Journal of Geophysical Research: Space Physics*, *123*(7), 5528–5537. https://doi.org/10.1029/2018JA025637

Zou, S., Moldwin, M. B., Coster, A., Lyons, L. R., & Nicolls, M. J. (2011). GPS TEC observations of dynamics of the mid-latitude trough during substorms. *Geophysical Research Letters*, *38*(14), L14109. https://doi.org/10.1029/2011GL048178